



HAL
open science

Satellite radar altimetry water elevations performance over a 200 m wide river: Evaluation over the Garonne River

Sylvain Biancamaria, Frédéric Frappart, A.-S Leleu, Vincent Marieu, D. Blumstein, Jean-Damien Desjonquères, F. Boy, Aldo Sottolichio, A. Valle-Levinson

► To cite this version:

Sylvain Biancamaria, Frédéric Frappart, A.-S Leleu, Vincent Marieu, D. Blumstein, et al.. Satellite radar altimetry water elevations performance over a 200 m wide river: Evaluation over the Garonne River. *Advances in Space Research*, 2017, 59 (1), pp.128-146. 10.1016/j.asr.2016.10.008 . hal-02136987

HAL Id: hal-02136987

<https://hal.science/hal-02136987>

Submitted on 22 May 2019

HAL is a multi-disciplinary open access archive for the deposit and dissemination of scientific research documents, whether they are published or not. The documents may come from teaching and research institutions in France or abroad, or from public or private research centers.

L'archive ouverte pluridisciplinaire **HAL**, est destinée au dépôt et à la diffusion de documents scientifiques de niveau recherche, publiés ou non, émanant des établissements d'enseignement et de recherche français ou étrangers, des laboratoires publics ou privés.

1 **Satellite radar altimetry water elevations performance over a 200 m wide river: evaluation**
2 **over the Garonne River**

3
4 S. Biancamaria^{1*}, F. Frappart^{1,2}, A.-S. Leleu¹, V. Marieu³, D. Blumstein^{1,4}, Jean-Damien
5 Desjonquères⁴, F. Boy⁴, A. Sottolichio³, A. Valle-Levinson⁵

6
7 ¹ LEGOS, Université de Toulouse, CNES, CNRS, IRD, UPS - 14 avenue Edouard Belin, 31400
8 Toulouse, France

9 Email addresses: sylvain.biancamaria@legos.obs-mip.fr; anne-sophie.leleu@legos.obs-mip.fr;
10 denis.blumstein@cnes.fr

11 ² GET, Université de Toulouse, CNRS, IRD, UPS - 14 avenue Edouard Belin, 31400 Toulouse,
12 France

13 Email address: Frederic.frappart@get.obs-mip.fr

14 ³ EPOC, Université de Bordeaux, CNRS - Bâtiment B18, allée Geoffroy Saint-Hilaire, CS 50023,
15 33615 Pessac Cedex, France

16 Email addresses: v.mariieu@epoc.u-bordeaux1.fr; a.sottolichio@epoc.u-bordeaux1.fr

17 ⁴ CNES - 18 avenue Edouard Belin, 31401 Toulouse Cedex, France

18 Email addresses: jean-damien.desjonqueres@cnes.fr; francois.boy@cnes.fr

19 ⁵ University of Florida, Civil and Coastal Engineering Department, Gainesville, FL 32611, USA

20 Email address: arnoldo@ufl.edu

21
22 * Corresponding author – email sylvain.biancamaria@legos.obs-mip.fr - phone: +33561332915

23
24 Published in Advances in Space Research, doi:10.1016/j.asr.2016.10.008

25 **Abstract**

26 For at least 20 years, nadir altimetry satellite missions have been successfully used to first
27 monitor the surface elevation of oceans and, shortly after, of large rivers and lakes . For the last 5-
28 10 years, few studies have demonstrated the possibility to also observe smaller water bodies than
29 previously thought feasible (river smaller than 500 m wide and lake below 10 km²). The present
30 study aims at quantifying the nadir altimetry performance over a medium river (200 m or lower
31 wide) with a pluvio-nival regime in a temperate climate (the Garonne River, France). Three
32 altimetry missions have been considered: ENVISAT (from 2002 to 2010), Jason-2 (from 2008 to
33 2014) and SARAL (from 2013 to 2014).

34 Compared to nearby in situ gages, ENVISAT and Jason-2 observations over the lower Garonne
35 River mainstream (110 km upstream of the estuary) have the smallest errors, with water elevation
36 anomalies root mean square errors (RMSE) around 50 cm and 20 cm, respectively. The few
37 ENVISAT upstream measurements have RMSE ranging from 80 cm to 160 cm. Over the estuary,
38 ENVISAT and SARAL water elevation anomalies RMSE are around 30 cm and 10 cm, respectively.
39 The most recent altimetry mission, SARAL, does not provide river elevation measurements for
40 most satellite overflights of the river mainstream. The altimeter remains “locked” on the top of
41 surrounding hilly areas and does not observe the steep-sided river valley, which could be 50 m to
42 100 m lower. This phenomenon is also observed, for fewer dates, on Jason-2 and ENVISAT
43 measurements. In these cases, the measurement is not “erroneous”, it just does not correspond to
44 water elevation of the river that is covered by the satellite. ENVISAT is less prone to get ‘locked’ on
45 the top of the topography due to some differences in the instrument measurement parameters,
46 trading lower accuracy for more useful measurements. Such problems are specific to continental
47 surfaces (or near the coasts), but are not observed over the open oceans, which are flatter.

48 To overcome this issue, an experimental instrument operating mode, called the
49 DIODE/DEM tracking mode, has been developed by CNES (Centre National d’Etudes Spatiales)
50 and has been tested during few Jason-2 cycles and during the first SARAL/AltiKA cycle. This

51 tracking mode “forces” the instrument to observe a target of interest, i.e. water bodies. The example
52 of the Garonne River shows, for one SARAL ground track, the benefit of the DIODE/DEM tracking
53 mode for a steep-sided river reach, which is not detected using the nominal instrument operating
54 mode. Yet, this mode relies on ancillary datasets (a priori global DEM and global land/water mask),
55 which are critical to obtain river valley observation. The ultimately computed elevations along the
56 satellite tracks, loaded on board, should have an absolute vertical accuracy around 10 m (or better).
57 This case also shows, when the instrument is correctly observing the river valley, that the altimeter
58 can detect water bodies narrower than 100 m (like an artificial canal).

59

60 In agreement with recent studies, this work shows that altimeter missions can provide useful
61 water elevation measurements over a 200 m wide river with RMSE as low as 50 cm and 20 cm, for
62 ENVISAT and Jason-2 respectively. The seasonal cycle can be observed with the temporal sampling
63 of these missions (35 days and 10 days, respectively), but short term events, like flood events, are
64 most of the time not observed. It also illustrates that altimeter capability to observe a river is highly
65 dependent of the surrounding topography, the observation configuration, previous measurements
66 and the instrument design. Therefore, it is not possible to generalize at global scale the minimum
67 river width that could be seen by altimeters.

68 This study analyzes, for the first time, the potential of the experimental DIODE/DEM
69 tracking mode to observe steep-sided narrow river valleys, which are frequently missed with
70 nominal tracking mode. For such case, using the DIODE/DEM mode could provide water elevation
71 measurements, as long as the on board DEM is accurate enough. This mode should provide many
72 more valid measurements over steep-sided rivers than currently observed.

73

74 **Keywords:** satellite altimetry; Garonne River; DIODE/DEM mode; ENVISAT; Jason-2; SARAL

75

76 **1. Introduction**

77 Continental waters play a key role in the Earth water cycle and are subject to complex
78 interactions at the interface between the atmosphere and ocean. These waters directly impact human
79 societies through food consumption, agriculture, and industrial activities. Continental waters need to
80 be monitored, especially during flood or drought events. They are also directly impacted by human
81 activities, through pumping, river embankment, dams, reservoirs, and hydraulic infrastructure. The
82 monitoring of the spatial distribution and temporal variability of surface waters still remains
83 challenging: there could be around 117 million of water bodies with an area above 0.002 km² on the
84 continental surfaces according to a recent study (Verpoorter et al., 2014). The biggest lakes and
85 rivers are of course important to the study of global hydrological process and water/carbon cycles.
86 But smaller lakes and rivers begin to draw attention, as they might also play a non-negligible role
87 because of their numbers (e.g. Downing et al., 2010). In situ monitoring of water bodies at global or
88 even regional scales is very heterogeneous, as it depends on local gage networks,. Moreover, in situ
89 measurements are considered sensitive information and are not always freely available to the
90 research community. In this context, satellite measurements are a viable complementary source of
91 information and especially those from nadir altimeters, even if they will not replace in situ
92 measurements.

93 Initially designed to monitor the dynamic topography of the ocean, satellite radar altimeters
94 have proven their abilities to observe continental surfaces water bodies elevations, allowing long-
95 term observations of water level variations of lakes (e.g., Birkett, 1995; Ponchaut and Cazenave,
96 1998; Medina et al., 2008; Crétaux et al., 2011; 2015), rivers (e.g., Birkett, 1998; Frappart et al.,
97 2006a; Santos da Silva et al., 2010; Biancamaria et al., 2011; Michailovsky et al., 2012) and
98 floodplains (e.g., Frappart et al., 2005; 2006b; 2012; Lee et al., 2009; Santos da Silva et al., 2010).
99 As altimetry measurements demonstrated their abilities to provide reliable water stages over large
100 water bodies, they started to be used with or to substitute missing in situ data, especially in large
101 remote river basins. Major hydrological applications are currently the followings: calibration of
102 hydrodynamics models (e.g., Wilson et al., 2007; Getirana, 2010; Yamazaki et al., 2012; Paiva et al.,

103 2013), estimate of discharge using either rating curves (e.g., Kouraev et al., 2004; Papa et al., 2012),
104 routing models (e.g., León et al., 2006; Hossain et al., 2014; Michailovsky and Bauer-Gottwein,
105 2014), or coupling with measurements of river velocities from multi-spectral images (e.g.,
106 Tarpanelli et al., 2015), estimate of surface water storage in large river basins (e.g., Frappart et al.,
107 2012; 2015a), lakes and reservoirs storage dynamics (e.g. Crétaux et al., 2016) and low water maps
108 of the groundwater table (Pfeffer et al., 2014). Nadir altimetry is quite a mature technology, as the
109 very first scientific altimeters flew more than thirty years ago. Continuity of measurements in time
110 is guaranteed by incoming follow-on missions like Jason-3 (launched 17 January 2016), Sentinel-
111 3A (launched 16 February 2016), Sentinel-3B (currently planned for 2017), Sentinel-3C and -3D
112 (which should be launched around 2021; ESA, 2016) and Jason-Continuity of Service/Sentinel-6 (in
113 2020 for Jason-CS A and 2026 for Jason-CS B; Scharroo et al., 2015).

114 Radar altimetry, however, has several limitations for monitoring land hydrology. The main
115 restrictions are its low spatial (one measurement every 175 to 400 m along track, for an instrument
116 footprint with several kilometers radius and an intertrack distance at the equator between 80 km to
117 315 km, depending on the mission) and temporal resolutions (repeat cycle of 10 days for
118 Topex/Poseidon and Jason-1/2/3 missions and 35 days for ERS-1&2, ENVISAT and SARAL, 27
119 days for Sentinel-3 missions). Because of these limitations, the use of altimetry data has been
120 limited to large (tens of km wide or wider) water bodies. Moreover, altimeters miss most water level
121 extrema during extreme flow periods or fail to study rapid hydrological events such as flash floods.
122 However, the altimeter performance depends not only on river size but also on the surrounding
123 topography (better performance over flat areas), on other surrounding water bodies and, to some
124 extent, on vegetation that will affect the reflected electromagnetic wave (Frappart et al., 2005;
125 Frappart et al. 2006a; Frappart et al., 2006b; Santos da Silva et al., 2010; Crétaux et al., 2011; Ricko
126 et al., 2012).

127 Improvements in nadir altimetry sensors performance, in the quality of the corrections
128 applied to the altimetry range and in measurements post-processing have allowed measurements of

129 water stage variations over small-to-medium rivers and small lakes. Small rivers are 40 to 200 m
130 wide, while medium rivers have widths between 200 and 800 m. Small rivers discharge from 10 to
131 $100 \text{ m}^3 \cdot \text{s}^{-1}$ while medium range between 100 and $1000 \text{ m}^3 \cdot \text{s}^{-1}$ (Meybeck et al., 1996). For lakes,
132 small lakes have areas $<0.01 \text{ km}^2$ (Verpoorter et al., 2014). On the basis of a global inventory of
133 lakes from optical satellite images, Verpoorter et al. (2014) showed that small lakes are the most
134 numerous (90 million, from a total of 117 million lakes worldwide), but cover a total area (0.27% of
135 non-glaciated land surfaces) much smaller than bigger lakes (which cover a total of 3.5%). Despite
136 their importance for land hydrology and water resources management, a large number of rivers and
137 lakes are poorly gaged (Alsdorf and Lettenmeier, 2003). Few studies have demonstrated the
138 possibility to accurately monitor water levels of small water bodies (e.g., Santos da Silva et al.,
139 2010; Michailovsky et al., 2012; Baup et al., 2014; Frappart et al., 2015a; Sulistioadi et al., 2015).
140 The present study aims at doing this benchmarking for a medium river: the Garonne River in
141 France. Section 2 presents the study domain, in situ gages and radar altimetry missions used.
142 Section 3 compares in situ and altimetry water elevations along the river main course and its
143 estuary, discuss the sources of errors and investigate potential solution for future altimetry missions
144 to improve measurements. Conclusions and perspectives are provided in section 4.

145

146 **2. Study domain and Methodology**

147

148 **2.1. Garonne River basin presentation and available data**

149

150 The Garonne River (Figure 1) is located in Southwest France and drains an area of 56,000
151 km^2 . Its mean annual discharge near its outlet, at Tonneins where the river width is around 200 m
152 (Figure 1), is around $600 \text{ m}^3 \cdot \text{s}^{-1}$. At the global scale, according to the Global Runoff Data Center
153 (GRDC) discharge database, it is the 120th largest river in the world by its annual discharge and the
154 3rd in mainland France. It is therefore a medium river according to Meybeck et al. (1996) (section
155 1).

156 The Garonne River has a pluvio-nival regime, with a low flow period between July and

157 October and high flow period between December and April. The river source is located in the
158 Pyrénées Mountains (South of the basin, Figure 1) and outflows to the Atlantic Ocean via the
159 Gironde estuary. The Garonne supports an agricultural activity that uses 70% of the total water
160 uptake (mainly from surface waters) during low flow period (Sauquet et al., 2009; Martin et al.,
161 2016). For more details on the Garonne basin, see Martin et al. (2016).

162 Water level and discharge gages on most rivers in France are operated by regional public
163 agencies (DREAL – Directions Régionales de l'Environnement, de l'Aménagement et du Logement)
164 and all their measurements are collected by the Service Central de l'Hydrométéorologie et d'Appui à
165 la Prévision des Inondations (SCHAPI) within the national 'Banque Hydro' database
166 (<http://www.hydro.eaufrance.fr>). Four gages from this database have been used in this study
167 (Verdun-sur-Garonne, Lamagistère, Tonneins and Marmande, see Figure 1), as they are on the
168 Garonne mainstream and provide validated water level measurements. Data are available with a
169 non-uniform temporal resolution that depends on the water elevation stage (the median time step for
170 all gages in Figure 1 is below 1 hour). All gages have records starting before 01 January 1 2002 (the
171 first year of the oldest altimetry mission considered in this study, see section 2.2.3). Water elevation
172 time series used in this study end 31 December 2010 at Verdun-sur-Garonne, 02 April 2014 at
173 Lamagistère, 01 February 2015 at Tonneins and 28 March 2014 at Marmande. The river width is
174 around 130 m at Verdun-sur-Garonne, 150 m at Lamagistère and 200 m at Tonneins and Marmande.
175 Also, the 15 km reach of the Garonne just upstream of Lamagistère (from the upstream confluence,
176 at Malause, to Lamagistère) has multiple man made hydraulic infrastructures along the river. There
177 are five weirs within the reach and a "run-of-the-river" dam at Malause, which induce river slope
178 breaks. Thus, water elevation variations within this reach and, in particular, at the location of ENV-
179 773 virtual station (see Figure 1 for its location and section 2.2.4 for definition of virtual station),
180 might not be comparable to water elevation variations at Lamagistère gage. There is no similar
181 infrastructure (and no such slope break) near other in situ gages that might impact comparison with
182 altimeter measurements.

183 Moreover, a Digital Elevation Model (DEM) at 25 m horizontal resolution, with few meters
184 absolute vertical accuracy, is available over the entire mainland France to the research community
185 and provided by the Institut National de l'Information Géographique et Forestière (IGN,
186 <http://professionnels.ign.fr>), a French government agency which is “the official reference for
187 geographic and forest information in France” (from <http://www.ign.fr/institut/en>).
188 Time series for three tide gages are also available on the Gironde estuary, seaward of the Garonne
189 (Figure 1). They are operated by the Service Hydrographique et Océanique de la Marine (SHOM –
190 <http://refmar.shom.fr>) for the Royan gage (from 19 September 2008 to 31 August 2014) and by the
191 Grand Port Maritime de Bordeaux for Port-Bloc (from 1 January 2006 to 12 October 2014) and
192 Richard (from 1 January 2006 to 31 December 2014) gages, with water level measurements every
193 minute.

194 All elevations (from gages time series and DEM) are referenced to the “Nouveau
195 Géoréféntiel Français” (NGF-IGN69), the official French vertical reference for the main territory.
196 Because all these data are available, the Garonne River basin is particularly well suited to evaluate
197 the capability of nadir altimeters to observe a medium river between 100 m and 200 m wide.

198

199 **2.2. Satellite altimetry missions used**

200 **2.2.1 Principle of altimetry measurement**

201 The purpose of radar altimeters is to provide the height of the ground surface above a reference
202 ellipsoid. To do so, the altimeter emits a radar pulse and records the radar echo using a pulse
203 compression technique. This record, also known as a waveform, contains the value of the returned
204 power as a function of the distance between the radar and the reflectors. In this study, the term
205 “range” is equivalent to the distance from the instrument. For technical reasons, the altimeter does
206 not record all the power backscattered by all targets between the instrument and the lowest ground
207 elevation within the instrument footprint (all the possible ranges). It only samples a small subset of
208 these ranges, called the range window or tracking window, whose size is typically between 30 m

209 and 50 or 64 m depending on the instrument, but can reach 1024 m for Envisat in the 20 MHz
 210 mode. For more details, see Benveniste et al. (2001), Desjonquères et al. (2010) and Steunou et al.
 211 (2015). A special function of the altimeter is to keep the range window tracking the ground surface
 212 (see section 2.2.2 for more information related to the on-board tracking system).

213 The two-way travel-time from the satellite to the surface is the measurement that needs to be
 214 estimated as accurately as possible from the waveform. It corresponds to an instant known, in the
 215 waveform, as the middle of the leading edge over the ocean. Over other types of surface, this time is
 216 more complex to retrieve and depends of the retracking algorithm used. It is accurately determined
 217 by the mission ground segment using retracking algorithms and is used to compute the distance
 218 between the satellite and the Earth surface, the altimeter range (R). Then, the satellite altitude (H)
 219 referenced to an ellipsoid is computed from orbit modeling, with an accuracy better than 2 cm (e.g.
 220 Cerri et al., 2010; Couhert et al., 2015; Dettmering et al., 2015).

221 Taking into account propagation corrections caused by delays from the interactions of
 222 electromagnetic waves in the atmosphere, and geophysical corrections, the height of the reflecting
 223 surface (h) with reference to an ellipsoid can be estimated as:

$$224 \quad h = H - \left(R + \sum(\Delta R_{propagation} + \Delta R_{geophysical}) \right) \quad (1)$$

225 where H is the satellite centre of mass height above the ellipsoid, estimated using the precise orbit
 226 determination (POD) technique, R is the nadir altimeter range from the satellite center of mass to
 227 the surface taking into account instrument corrections, $\sum \Delta R_{propagation}$ is the sum of the
 228 geophysical and environmental corrections applied to the range, respectively, and $\sum \Delta R_{geophysical}$ is
 229 another geophysical correction. Furthermore, $\sum \Delta R_{propagation}$ is computed as follow:

$$230 \quad \sum \Delta R_{propagation} = \Delta R_{ion} + \Delta R_{dry} + \Delta R_{wet} \quad (2)$$

231 where ΔR_{ion} is the atmospheric refraction range delay due to the free electron content associated
 232 with the dielectric properties of the ionosphere, ΔR_{dry} is the atmospheric refraction range delay due
 233 to the dry gas component of the troposphere, ΔR_{wet} is the atmospheric refraction range delay due to
 234 the water vapor and the cloud liquid water content of the troposphere. Also, $\sum \Delta R_{geophysical}$

235 corresponds to the following corrections:

$$236 \quad \sum \Delta R_{geophysical} = \Delta R_{solid\ Earth} + \Delta R_{pole} \quad (3)$$

237 where $\Delta R_{solid\ Earth}$ and ΔR_{pole} are the corrections accounting for crustal vertical motions due to the
238 solid Earth and pole tides, respectively. Over the ocean, other corrections need to be applied to take
239 into account other physical processes (such as ocean tides, see Chelton et al., 2001, for more
240 information).

241

242 **2.2.2 On board tracking system**

243 As indicated in the previous section, one important function of the altimeter is to modify the
244 position of its tracking window to make it follow the ground topography, which can rapidly change
245 over few kilometers on the continents. This is automatically performed on board in “closed-loop”
246 by the Adaptive Tracking Unit (ATU) from previously received waveforms. Chelton et al. (2001)
247 and Desjonquères et al. (2010) provide a detailed description of the closed-loop tracking system for
248 TOPEX and Poseidon-3 altimeters, respectively. The following paragraph provides only a
249 simplified overview, which is sufficient enough to understand the observations presented in this
250 study.

251 The principle of the closed loop is that the ATU tries to keep some signal in its tracking
252 window. On Poseidon-3, this is done by using the so-called “median mode” (Desjonquères, 2010),
253 which tries constantly to center the signal in the window. If this fails, the level of received signal
254 decreases dramatically. When the level of received signal becomes lower than a predefined
255 threshold, the ATU considers that the tracking is lost and switches to a “search” mode in which it
256 scans a window, with range of a few kilometers range, centered on the estimated satellite altitude.
257 The scan begins with the smallest range (i.e. closest to the satellite) and the tracking window is
258 moved until the level of received signal exceeds again another specified threshold (Desjonquères et
259 al., 2010).

260 This behavior implies that the ground surface observed by nadir altimeters heavily depends

261 on the previously received radar echoes. For example, the geometry of the observations can induce
262 loss of radar echoes tracking in some circumstances (e.g., if the satellite trajectory crosses a steep-
263 sided valley perpendicularly) or not, (e.g., if it follows the valley over a long distance). In general,
264 when the tracking is lost and the ATU is in search mode, the signal received from the top of the hills
265 is high enough to exceed the threshold making the ATU to stop the search. This can occur before the
266 tracking window reaches the river that flows in the valley, but of course this depends on the depth
267 of the valley as well as the size of the tracking window. So the top of the hilly areas often tends to
268 be observed rather than rivers in the valley. However the exact behavior of the altimeter depends on
269 the ground reflectivity, the size of the tracking window and the two thresholds mentioned above.
270 Thus, whenever there are variations of topography, there is no way to control which part of the
271 scenery will be observed by the radar altimeter in the closed-loop tracking mode.

272 To overcome this challenge, a new tracking mode, the Doris Immediate Orbit on board
273 DEtermination/Digital Elevation Model (DIODE/DEM) mode, has been implemented on board
274 Poseidon-3 and AltiKa altimeters. In this mode, tracking range is not estimated in closed-loop, but
275 in “open-loop”. In this case, the satellite/ground range is not estimated automatically from formerly
276 measured signal, but using a DEM stored on board and an estimate of the satellite orbital position,
277 computed on board and in real time by the DIODE navigator function of the DORIS (Doppler
278 Orbitography and Radio-positioning Integrated by Satellite) instrument (Desjonquères et al., 2010).
279 The DEM mode was activated during cycles 3, 5, 7, 34, 209 and 220 for Jason-2 and only during a
280 portion of SARAL cycle 1 (tracks 600 to 800 from 4 April to 10 April 2013), corresponding to
281 tracks 646 and 773 over the Garonne basin (see Figure 1 for their location). To compute on board
282 elevations used by the DIODE/DEM tracking mode, CNES used an a priori global DEM and a
283 global land/water classification (Desjonquères, 2009). If there is water in the land/water
284 classification within the instrument footprint, then only a priori DEM elevations within the water
285 mask are used to compute on board elevation (Desjonquères, 2009). However, if there is no water,
286 then all land elevations are considered. Therefore, for steep-sided regions with no water in the

287 classification (or if the water mask is not correctly geolocalized), the computed on board elevations
288 can be closer to the top of the hills elevations than the river valley elevations. Furthermore, the
289 waveform is expected to be centered on the first third of the tracking window. As this window size
290 is around 50 m for Jason-2 and 30 m for SARAL, it has been estimated that the a priori DEM
291 accuracy should be around 10 m (even slightly less for SARAL).

292 For Jason-2, the a priori global DEM used is the 1 km Altimetry Corrected Elevation DEM
293 (ACE; Berry et al., 2000) and the water mask comes from the Generic Mapping Tools (GMT,
294 <http://gmt.soest.hawaii.edu/>) (Desjonquères, 2009). A comparison between ACE DEM and 25 m
295 IGN DEM (see section 2.1) tends to show that ACE accuracy over the Garonne valley is better than
296 10 m. Global-scale ACE uses local Digital Terrain Elevation Data (DTED) and altimetry data from
297 the ERS-1 (European Remote Sensing-1 satellite) acquired during its geodetic mission. However,
298 over the Garonne River valley, ACE elevations come only from DTED (exact source is not provided
299 in the ACE documentation). In addition, the river position in the GMT database is not correctly
300 geolocalized. Therefore, the on board elevations over the Garonne might be biased toward
301 elevations on top of the hills. For SARAL, the a priori global DEM corresponds to ACE2 (Berry et
302 al., 2010) and the land/water mask is derived from Globcover
303 (http://due.esrin.esa.int/page_globcover.php). The accuracy of ACE2 also seems to be better than 10
304 m over the Garonne valley. Globcover correctly geolocalizes the Garonne River but because of its
305 300 m pixel size and the undersampling to 1 km pixels in the CNES tool, pixels identified as water
306 do not always correspond to the river surface. These discrepancies can impact the computed
307 elevations stored on board.

308 Birkett and Beckley (2010) evaluated both the closed-loop and the DIODE/DEM modes (for
309 cycles 3, 5, 7 and 34) for Jason-2 over 28 lakes and reservoirs around the world with areas spanning
310 from 380,000 km² (Caspian Sea, Kazakhstan) to 150 km² (Windsor lake, Bahamas). They
311 concluded that both modes on Jason-2 are able to monitor water bodies with area around 150 km²
312 and width around 0.8 km. This monitoring capability is an improvement compared to

313 Topex/Poseidon and Jason-1, with the DIODE/DEM having the fastest acquisition time for many
314 targets. However, for few targets (Chajih lake, 900 km², Windsor lake, 150 km², Brokopondo
315 reservoir 1,500 km² and Powell and Diefenbaker reservoir systems, 500 km² and 550 km²,
316 respectively), they noted some loss of data in the DIODE/DEM mode for cycles 3, 5 and 7, whereas
317 the closed-loop mode was performing well during other cycles. These targets are better (at least
318 partially) observed during cycle 34, after the on board DEM elevations have been updated and some
319 altimeter parameters have been tuned in cycle 16. They attributed errors to “inadequate resolution
320 and/or data in the DEM” and concluded that the on board DEM might not be “optimized for all
321 regions”. For all investigated lakes and reservoirs, they observed some cases where the closed-loop
322 successfully observed the water body, contrarily to the DIODE/DEM. For all other cases, both
323 tracking modes provided similar results (both failed or succeeded to observe water bodies). But
324 there was no case where the DIODE/DEM mode observed the target and the closed-loop did not.
325 However, Birkett and Beckley (2010) considered in their study targets that were larger than the
326 Garonne River.

327

328 **2.2.3 Altimetry datasets**

329 This study uses altimetry missions only after 2002, namely the ENVironmental SATellite
330 (ENVISAT) mission from the European Space Agency (ESA), Jason-2 mission from National
331 Aeronautics and Space Administration (NASA) and Centre National d'Etudes Spatiales (CNES),
332 and Satellite for ARGos and ALtika (SARAL)/Altimeter in Ka-Band (AlitKa) mission jointly
333 developed by the Indian Space Research Organization (ISRO) and CNES. Table 1 sums up the main
334 characteristics and technical details of these three altimetry missions, which are described in more
335 detail below.

336 ENVISAT mission was launched by ESA on 01 March 2002. It carried 10 instruments
337 including the advanced radar altimeter (RA-2). It was based on the heritage of sensors on board the
338 European Remote Sensing (ERS-1 and 2) satellites. Altimeter RA-2 was a nadir-looking pulse-

339 limited radar altimeter operating at two frequencies: Ku- (13.575 GHz), as ERS-1 and 2, and S- (3.2
340 GHz) bands. Its goal was to collect radar altimetry over ocean, land and ice caps (Zelli, 1999).
341 Altimeter RA-2 could change the range resolution to set the range detection window to three sizes:
342 1024 m, 256 m and 64 m (they are also commonly designated as 20MHz, 80MHz and 320MHz
343 modes, respectively, corresponding to the bandwidths used to achieve the corresponding window
344 width; Benveniste et al., 2001; ESA, 2007). Changing the tracking window is particularly useful
345 over continents to adapt tracking to ground topography changes (regions with rapidly varying
346 altitude will be better tracked with a relatively wider window, whereas flat regions will be more
347 precisely observed with a relatively narrower window). The range window is sampled using a fixed
348 number of bins (or gates). A bin corresponds to a continuous interval of ranges that will be
349 aggregated to a unique range value, during the analog-to-digital conversion step. Changes in range
350 window size are done automatically on board, based on the received signal and reference data
351 stored in the on board memory (ESA, 2007). ENVISAT orbited at an average altitude of 790 km,
352 with an inclination of 98.54°, on a sun-synchronous orbit with a 35-day repeat cycle. It provided
353 observations of the Earth surface (oceans and lands) from 82.4° latitude North to 82.4° latitude
354 South. This orbit was formerly used by ERS-1 and 2 missions, with an equatorial ground-track
355 spacing of about 80 km. ENVISAT remained on this nominal orbit until October 2010 and its
356 mission ended 08 April 2012. This study used ENVISAT data from cycles 6 (which started 14 May
357 2002) to 94 (which ended 21 October 2010).

358 Jason-2 mission was launched on 20 June 2008 as a cooperation between CNES,
359 EUMETSAT, NASA and NOAA. Its payload is mostly composed of the Poseidon-3 radar altimeter
360 from CNES, the Advanced Microwave Radiometer (AMR) from JPL/NASA, and a triple system for
361 precise orbit determination: the DORIS instrument from CNES, a GNSS receiver and a Laser
362 Retroreflector Array (LRA) from NASA. Jason-2 orbits at an altitude of 1336 km, with an inclination
363 of 66°, on a 10-day repeat cycle, providing observations of the Earth surface (oceans and lands)
364 from 66° latitude North to 66° latitude South, with an equatorial ground-track spacing of about 315

365 km. This orbit was formerly used by Topex/Poseidon, and Jason-1. Poseidon-3 radar altimeter is a
366 two-frequency altimeter, operating at Ku- (13.575 GHz) and C- (5.3 GHz) bands (Desjonquieres et
367 al., 2010). The tracker range window is the same as previous Poseidon instruments and has a useful
368 size around 50m (sampled over 104 range bins). Jason-2 measurements are used in this study from
369 cycle 1 (which started 12 July 2008) to cycle 227 (which ended 09 September 2014) h. Jason-2 raw
370 data are processed by SSALTO (Segment Sol multimissions d'ALTimétrie, d'Orbitographie).

371 SARAL is a CNES-ISRO joint-mission that was launched on 25 February 2013. Its payload
372 is composed of the AltiKa radar altimeter and bi-frequency radiometer, and a double system for
373 precise orbit determination (Steunou et al., 2015): DORIS instrument and a Laser Retroreflector
374 Array (LRA). SARAL flights on the same nominal orbit than ENVISAT (see above). AltiKa radar
375 altimeter is a mono-frequency altimeter and the first one to operate at Ka-band (35.75 GHz). The
376 bandwidth of the signal has been increased (480 MHz of useful bandwidth; Sengenés and Steunou,
377 2011) with respect to Jason-2 and ENVISAT, improving the range resolution. As the number of
378 useful bins remains the same as for the Jason altimeters (104 bins), the tracker window size is
379 around 30 m. For electromagnetic wave in Ka-band, ionospheric delay becomes negligible. In this
380 study, SARAL/AltiKa measurements from cycle 1 (which started 14 March 2013) to cycle 17
381 (which ended 30 October 2014) have been used.

382 Altimetry data processed in this study come from the Geophysical Data Records (GDRs) –
383 GDR T patch 2 for SARAL, GDR v2.1 for ENVISAT, GDR D for Jason-2, delivered by
384 CNES/ESA/NASA processing centers. Since this study has been performed, a new Jason-2 GDR
385 version has been released in May 2015 (GDR E). Differences between GDR D and E are expected
386 to have a low impact on the results presented here, as the foreseen improvement is a better
387 agreement of the geographically correlated radial orbit drift rate (1 mm/year to less than 0.5
388 mm/year over roughly 6 years) with respect to JPL (RLSE14A) GPS-only reduced-dynamic orbits
389 for Jason-2 (for more details, see
390 http://www.aviso.altimetry.fr/fileadmin/documents/data/tools/New_GDR_E_orbit_20150521.pdf).

391 Similarly, a new SARAL GRD E is now available. But SARAL GDR T patch 2 and SARAL GDR
392 E must provide similar results for this study. These data are provided in a consistent NetCDF
393 (Network Common Data Form) format with coherent geophysical corrections for all missions by
394 Centre de Topographie de l'Océan et de l'Hydrosphère (CTOH –<http://ctoh.legos.obs-mip.fr/>). They
395 are sampled along the altimeter track at 18, 20 and 40 Hz for ENVISAT, Jason-2 and SARAL
396 respectively. As explained in the previous section, a so-called retracker algorithm is needed to
397 estimate the satellite/ground range R (Eq. 1) and the surface backscattering coefficient from the
398 received electromagnetic signal. Previous studies showed that Ice-1 retracking algorithm (Wingham
399 et al., 1986) is one of the most suitable for hydrological studies, in terms of accuracy of water levels
400 and availability of the data (e.g. Frappart et al., 2006a; Santos da Silva et al., 2010), among the
401 commonly available retracked data present in the GDRs. However, Santos da Silva et al. (2010)
402 found, on the Amazon basin, that Ice-2 retracking algorithm (Legrésy and Rémy, 1997) could
403 provide similar results to Ice-1. Sulistioadi et al. (2015) showed, for some 250 m wide Indonesian
404 river reaches, that Sea Ice retracking algorithm (Laxon, 1994) can provide, in some cases, slightly
405 more accurate water levels than Ice-1. In the following, when not explicitly indicated, ranges used
406 to derive altimeter heights and backscattering coefficients are those derived from the Ice-1
407 retracking algorithm. ENVISAT GDRs directly provide ranges estimated using Ice-1 and Sea Ice
408 algorithms. Therefore, in section 3.1, a comparison is presented between Ice-1 and Sea Ice derived
409 water heights for ENVISAT measurements. Ice-2 retracker has not been considered as it provides
410 similar results to Ice-1 (Santos da Silva et al., 2010). Similarly, the retracker used over ocean
411 (Brown, 1977) has not been used, as it has been widely shown that it provides the worst results
412 compared to the three other retracking algorithms for rivers (e. g. Frappart et al., 2006a; Santos da
413 Silva et al., 2010; Sulistioadi et al., 2015).

414 Over the ocean, wet troposphere corrections are computed from the on board radiometer
415 measurements, for each altimetry mission. However, measurements over continents from these
416 radiometers cannot be used to estimate those corrections, as the ground emissivity (contrarily to

417 water) is much more important than the emissivity from the atmosphere. In this case, the
418 propagation corrections applied to the range are derived from the Era Interim model outputs by the
419 European Centre Medium-Range Weather Forecasts (ECMWF) for the dry/wet troposphere range
420 delays. The range correction accounting for ionosphere delays is estimated using the Global
421 Ionospheric Maps (GIM).

422

423 **2.2.4 Time series of altimetry-based water levels**

424 Time variations of river levels from radar altimetry measurements are computed at virtual
425 stations. A virtual station is defined as the intersection between an orbit ground track and a water
426 body (*i.e.*, lake, reservoir river channel, floodplain or wetland). At these specific locations,
427 variations from one cycle to the next of height h , derived from altimeter measurements (see Eq. 1),
428 can be associated to changes in water level.

429 In this study, we used the Multi-mission Altimetry Processing Software (MAPS) that allows a
430 refined selection of the valid altimetry data to build virtual stations (Frappart et al., 2015b). Data
431 processing is composed of three main steps: a coarse delineation of the virtual stations using Google
432 Earth, a refined selection of the valid altimetry data, and a computation of the water level time-
433 series. For virtual stations on the Garonne mainstream (Figure 1), the length of the selection is not
434 constant and varies from 700 m to 2 km. The altimetry-based water level is computed for each cycle
435 using the median of the selected altimetry heights, along with their respective deviation (*i.e.*, mean
436 absolute deviations). This process is repeated each cycle to construct the water level time series at
437 the virtual stations.

438

439 **3. Results**

440 **3.1. Multi-satellite water elevation on the Garonne River mainstream**

441 The altimetry-based time series of water elevation at virtual stations shown on Figure 1 have
442 been compared to the closest in situ station available in the Banque Hydro database (see section

443 2.1), with the exception of virtual stations JA2-070a and JA2-070b. They have not been used in this
444 study, as the confluence with the Lot River (one of the main Garonne River tributaries) is located
445 between the closest in situ gage (Tonneins) and the virtual stations. Therefore water elevation at the
446 gage might not be representative of water elevation at the virtual stations.

447 For other virtual stations, only common dates have been used for the comparison between
448 altimetry and in situ time series. In situ measurements recorded the same day as the altimetry
449 measurement are linearly interpolated at the altimetry measurement observation time. If there is no
450 in situ measurement the same day as the altimetry observation, this observation is not considered. In
451 situ time series have been referenced to UTC (Coordinated Universal Time) to match the altimeter
452 time reference. Elevation anomaly time series have been computed for both the altimeters and in
453 situ gages. The anomalies are computed by removing, from the elevation time series, its temporal
454 mean over the same common dates between in situ and altimetry time series (e.g. Biancamaria et
455 al., 2011).

456 Table 2 shows the correlation coefficient, mean bias (mean of the difference) and Root Mean
457 Square Error (RMSE) between altimetry and in situ time series for both absolute water elevations
458 referenced to NGF-IGN69 and water elevation anomalies, along the Garonne River mainstream. For
459 anomaly time series, the Nash-Sutcliffe (NS) coefficient (Nash and Sutcliffe, 1970) is also
460 computed. The NS coefficient, which ranges between $-\infty$ and 1, is widely used to assess how an
461 estimated time series (most of the time from a model) accurately match (i.e., in time and amplitude)
462 in situ measurements. The closer to 1 the NS coefficient is, the closest to the in situ time series the
463 altimetry-based water elevations are. NS above 0.5 can be considered satisfactory (Moriassi et al.,
464 2007). However, a negative NS means that the estimated time series is a worse “predictor” than the
465 in situ time series mean and should be considered as unacceptable (Moriassi et al., 2007). In this
466 study, the NS is not computed for absolute water elevation (bias between absolute in situ and
467 altimetry water elevation induces negative NS), but for their anomalies. Table 2 also provides
468 distance between the altimetry virtual station and the gage, number of common dates between

469 altimetry and in situ time series, and the amplitude (maximum minus minimum over the common
470 dates) of the in situ time series.

471 At Lamagistère and Verdun-sur-Garonne, ENVISAT data are not really correlated to the in
472 situ measurement and the NS coefficients are negative, indicating poor performance of the
473 altimeters. For virtual stations ENV-102 and ENV-773, which correspond to the worst results for
474 ENVISAT, the distance to the in situ gage can partially explain the mismatch. However, the small
475 river width (~150 m) and the surrounding topography affecting the quality of the altimetry signal
476 are also likely to be an important source of error. Virtual station ENV-646, which is only 1 km
477 downstream the gage at Lamagistère, has better RMSE (1.80 m for absolute water elevations and
478 0.80 for water elevation anomalies), correlation coefficient (0.61) and NS coefficient (-0.53)
479 compared to upstream ENVISAT virtual stations, even if they cannot be considered as satisfactory.

480 Downstream, at Tonneins and Marmande, where the river width is around 200 m, ENVISAT
481 altimetry time series are of good quality with correlation coefficient around 0.8, NS around 0.7 and
482 water elevation anomalies RMSE between 0.5 m and 0.6 m for ENVISAT. For ENVISAT and
483 Jason-2, the mean bias must be mostly explained by the river slope between the gage and the
484 altimetry virtual station, as they have the same order of magnitude as the slopes computed from
485 IGN DEM, even if the DEM vertical accuracy (few meters) prevents a quantitative estimate of the
486 river slope (which also varies in time). The sign of the bias depends of the position of the virtual
487 station compared to the gage (positive if the virtual station is downstream and negative if it is
488 upstream). Yet, some part of this bias might also be related to the altimeter measurement error.

489 Results shown in Table 2 have been computed using Ice-1 retracker algorithm and the
490 median value of altimetry heights for each observation time (see section 2.2.4). Even if some
491 studies reported better results using Ice-1 retracker (over the Amazon see Frappart et al., 2005;
492 Frappart et al., 2006a; Santos da Silva et al., 2010), Sulistioadi et al. (2015) found that Ice-1 was not
493 always providing the best results for some Indonesian rivers, whose widths were around 250 m. In
494 this study, the Sea Ice retracker was sometimes performing better than Ice-1. As ENVISAT GDRs

495 provide ranges computed using at least these two retracker algorithms, we computed water
496 elevation from both retrackers and compared them to in-situ measurements for ENVISAT virtual
497 stations along the Garonne mainstream. These results are shown in Table 3. Within each virtual
498 station, the median water elevation is computed for each observation time, as it is more robust than
499 the mean, when there are outliers (Frappart et al., 2005; Frappart et al., 2006a). However, Santos da
500 Silva et al. (2010) stated that computing both the median and the mean can provide a “qualitative
501 indicator of the presence of outliers”. That is why both the median and the mean are shown in Table
502 3. This table seems to confirm the results from Sulistioadi et al. (2015), the best results are not
503 always obtained with Ice-1. For the three virtual stations with NS coefficient below 0, two have
504 better results with Sea Ice. For the two virtual stations with NS coefficient above 0.5, one has better
505 results with Ice-1, the other with Sea Ice. However, for these two virtual stations, difference
506 between RMSE for these two retrackers is just a few centimeters, which is small compared the
507 actual value of the RMSE (more than 50 cm). Therefore, both retrackers are well suited for the
508 Garonne basin. Results using the median are better, most of the time, than results using the mean
509 (except for Ice-1 and virtual station ENV-315, where the RMSE using the mean is only 2 cm lower
510 than the RMSE using the median). From these results it seems that both the median Ice-1 and the
511 median Sea Ice are well suited for the Garonne basin. Differences between these two retrackers are
512 one order of magnitude lower than the RMSE obtained from comparison to in situ time series.

513 Figure 2 shows enlargements from Figure 1 on ENVISAT and Jason-2 virtual stations at
514 Lamagistère (a.), at Tonneins (b.) and in the estuary (c.). Especially, it should be recalled that there
515 are four weirs between ENV-773 virtual station and Lamagistère gage (as explained in section 2.1),
516 which are 10 km apart. These weirs cause slope breaks and can explain at least a part of the 1.55 m
517 water elevation anomalies RMSE for this virtual station. Figure 3 shows ENVISAT (red curves for
518 Ice-1 and cyan curves for Sea Ice) and in situ (blue curves) water elevation anomaly time series at
519 the satellite measurement times for virtual stations ENV-646 (Fig 3.a) and ENV-188 (Fi. 3.c). On
520 this figure, the right panels (b. and d.) show all records in the in situ water elevation anomalies time

521 series (blue dots) and the altimetry water elevation anomaly measurements (red dots for Ice-1 and
522 cyan dots for Sea Ice) during the common time period for these two virtual stations. These right
523 panels highlight the coarse altimetry time sampling. On Figure 3.d, ENVISAT seems to roughly
524 sample the water elevation seasonal cycle, but, because of the 35 days repeat orbit, it cannot
525 observe intra-monthly variability. This variability can be quite important for a medium river like the
526 Garonne, for which precipitation and snow melting induce few meters water elevation variations
527 within few days at Tonneins. Figure 3 corresponds to two virtual stations (ENV-646 and ENV-188)
528 for which Sea Ice retracker is performing better than Ice-1 retracker, yet the two retracker's time
529 series remain close. Table 3 shows that for two other virtual stations (ENV-773 and ENV-315) Ice-1
530 performs better than Sea Ice. This result is in agreement with the results obtained by Sulistioadi et
531 al. (2015): for medium size rivers, Ice-1 is not always the best retracker. However, water elevation
532 obtained from both retracker's are close enough and both could be used (there is just few centimeters
533 difference between them for the two virtual stations, which have a correlation coefficient above
534 0.8). According to these results and as Sea Ice retracker is not provided in Jason-2 GDRs, only
535 results using Ice-1 retracker will be shown in the following.

536 For Jason-2 virtual station JA2-070, in between Tonneins and Marmande, correlation
537 coefficient is equal to 0.98, NS around 0.95 and the RMSE of water elevation anomalies is close to
538 20 cm. Results for virtual stations JA2-035 show slightly lower agreement with a correlation
539 coefficient of 0.91 and water elevation anomalies RMSE and NS coefficient of 0.36 cm and 0.82,
540 respectively. The most noticeable feature in this virtual station is the few dates (62) that measure
541 river water commonly with the Marmande gage time series (Table 2). In comparison, virtual station
542 JA2-070 has 150 dates with measurements of river water elevation during the same period. For the
543 other dates, elevations are 50 m higher than valid measurements of river water elevations and have
544 therefore been removed during the virtual station time series generation before comparison with in
545 situ data. These dates (around 40 for JA2-070 and 140 for JA2-035) correspond to cases when the
546 altimeter remains 'locked' on the surrounding hills (see section 2.2.2 for an explanation of this

547 phenomenon). The Garonne valley is roughly 5 km or less wide at these locations and is surrounded
548 by hilly areas (see Figure 2) that can be 50 m to 100 m higher than the valley (according to the IGN
549 DEM and knowledge of the region). These two virtual stations also illustrate the importance of the
550 geometry of observation. The track 070 is almost parallel to the valley over a long distance (almost
551 30 km). Therefore, distance variations between the ground and the radar are much smoother
552 compared to the track 035 that crosses the valley almost orthogonally.

553 Figure 4 presents similar plots than Figure 3, but for the Jason-2 virtual station JA2-070,
554 using Ice-1 retracker only (red curves and red dots). This virtual station clearly shows better results
555 than ENVISAT virtual station ENV-188 (Figure 3.c and 3.d), when compared to Tonneins in situ
556 time series. Besides, with a 10 days repeat orbit, Jason-2 observes higher frequency variations, but
557 still misses all the local maxima and especially the 2009 and 2014 heavy floods, which lasted only
558 few days.

559 Table 2 also highlights high mean bias for most SARAL virtual stations, only virtual station
560 SRL-188 have correlation and errors similar to ENVISAT. For the three other ones, the mean error
561 goes from 44 m to 105 m, with few dates in the time series, indicating that the altimeter is not
562 observing the river valley but the surrounding hills. This problem is similar to that already observed
563 for Jason-2 time series. However, for these SARAL virtual stations and contrary to Jason-2 virtual
564 stations, there is no measurement on the river. ENVISAT is less affected by such effects, thanks to
565 its three resolutions (see section 2.2.3) and differences in the closed-loop parameters. This
566 drawback and potential reasons for the differences between the three missions is discussed in more
567 detail in section 3.2.

568 In the Gironde estuary, at Richard tide gage (see Figure 1 for its location), both ENVISAT
569 and SARAL tracks 274 compare unfavorably to in situ measurements (Table 4) with correlation
570 coefficients of 0.28 and 0.09, respectively. As the absolute vertical reference for this tide gage is not
571 known, mean bias and the absolute elevation RMSE cannot be computed. The RMSE of water
572 elevation anomalies is around 1.5 m. Differences between altimetry and in situ time series could be

573 related to instrument error, impact of surrounding lands and the fact that water elevation variations
574 at the tide gage might not be representative of water elevation variations along the satellite ground
575 track. Figure 5, shows the measured elevation from ENVISAT/RA2 for track 274 during 21 June
576 2007 (red line) and the IGN DEM elevation (green curve) on the estuary. It shows that over half of
577 the estuary, the altimeter remains locked over the surrounding topography (which is a common
578 issue for nadir altimetry due to the closed-loop tracking mode, as explained in section 2.2.2). These
579 measurements are not taken into account to compute time series for ENV-274, but represent a
580 source of error that is likely to affect the altimetry signal in the lower estuary.

581 Results are much better for both ENVISAT and SARAL tracks 859 (Table 4) at Port-Bloc
582 and Royan tide gages (see Figure 1 and 2.c for their locations). The correlation coefficient is above
583 0.97, water elevation anomalies RMSE are around 30 cm for ENVISAT and 10 cm for SARAL. The
584 comparison between anomalies time series measured by Port-Bloc tide gage and ENVISAT track
585 859 is shown on Figure 6.a and 6.b and SARAL track 859 on Figure 6.c and 6.d. Figures 6.b. and
586 6.d. also highlight the well-known effect of tidal aliasing in the altimeter water elevation time
587 series, due to the altimetry satellite orbit repeat period which is much higher than the tides period (e.
588 g. Le Provost, 2001). As stated by Le Provost (2001), the important difference between altimeter
589 time sampling (10 days or 35 days) and semidiurnal and diurnal tides period (between 12 to 24
590 hours), leads to alias these tides “into periods of several months to years”. But the issue of tidal
591 aliasing is beyond the scope of the present paper.

592

593 **3.2. Tracking issue and possible solution**

594 The challenge of observing the Garonne valley for some altimetry mission (SARAL/AltiKa,
595 but also Jason-2 and ENVISAT to a lower extent), highlighted in section 3.1, has multiple origins,
596 as explained in section 2.2.2. The Garonne valley is only 5 km wide at virtual stations ENV-/SRL-
597 773 and 50 m to 100 m lower than the surrounding hilly areas. Due to the closed-loop tracking
598 algorithm, nadir altimeter tends to get locked on the top of the hilly areas and miss steep-sided

599 valleys (see section 2.2.2). The portion of SARAL/AltiKa ground track that crosses the Garonne
600 valley (roughly perpendicularly, see Figure 2.a) is only 7 km long. As the antenna footprint on the
601 ground is equal to 4 km, considering the 3-dB aperture angle of 0.6° for SARAL that defines the
602 half-power points of the antenna radiation pattern (Steunou et al., 2015), the instrument still
603 receives some backscattered energy from the surrounding hilly areas for previous radar echoes
604 when it is near and over the valley. Therefore, the ATU does not change the position of the tracking
605 window, which remains locked on the hills. After few kilometers, the hills are not in the antenna
606 footprint anymore and no more energy is received, resulting in a loss of measurements. By the time
607 the instrument changes the tracking window position (search mode, see section 2.2.2) and receives
608 again some energy, acquisition of the Garonne valley has been lost. Figure 7 shows an example of
609 data loss by AltiKa due to the closed-loop. On this figure, the x-axis represents the latitude along
610 the SARAL track 773 (see Figure 2.a for its location) and the y-axis corresponds to elevation
611 referenced to NGF-IGN69. The green curve corresponds to the IGN DEM. The Garonne River
612 location is indicated by the blue rectangle. SARAL measurement for cycle 2 (in closed-loop) is
613 shown by the magenta dashed line. During cycle 2, AltiKa remains locked over the hills and loses
614 tracking over the Garonne valley, as previously explained.

615 Signal-locking over hills is less frequent for Jason-2 virtual station JA2-070, because of a
616 more favorable observation configuration than SARAL. Jason-2 track flies over the Garonne valley
617 and follows the river over 30 km before virtual station JA2-070. Therefore, elevation variations
618 observed by the satellite are smoother than SARAL. Smoother variations along Jason-2 track allow
619 more time for the closed-loop tracking algorithm to adapt to the hills/valley transition, whereas
620 ENVISAT and SARAL track 188 is almost perpendicular to the valley (Figure 2.b). Jason-2 virtual
621 station JA2-035 has a configuration of observation close to SARAL track 188, that is why it also
622 has few river water elevation measurements.

623 However, ENVISAT better performance compared to SARAL/AltiKa is not due to a different
624 observation configuration (contrary to Jason-2, as SARAL is on the same orbit), but it must be

625 related to the three window sizes that are chosen automatically on board (64 m, 256 m, 1024 m, see
626 section 2.2.3). ENVISAT is better suited to observe ground with appreciable slope variations as the
627 instrument increases the size of its tracking window, which allows measurements in the river valley.
628 Table 5 shows percentage of data for all ENVISAT cycles acquired with each window size, for all
629 virtual stations. Measurements for virtual stations close to high relief have more tracking window
630 size variability (typically the case of ENV-102, ENV-773 and ENV-315). At ENV-188 virtual
631 station, the river is more distant from high relief, the altimeter is very frequently in 320 MHz mode
632 (64 m window size) and that is also why it is the only SARAL/AltiKa virtual station observing river
633 water elevations. However, increasing the tracking window size (with the same number of range
634 bins) degrades the range resolution of the altimeter. Yet, SARAL better results over the estuary,
635 compared to ENVISAT, must be linked to its improved range resolution.

636 Nadir altimeters observe a ground surface most of the time but this surface is not always the
637 most useful for hydrologists. To overcome this issue and force the altimeter to observe the river
638 valley instead of the surrounding hilly areas, the DIODE/DEM tracking mode has been developed
639 by CNES (see section 2.2.2). SARAL/AltiKa measurements for virtual station SRL-773 were
640 performed in DIODE/DEM mode during the first cycle of the mission and they are shown in Figure
641 7 (red curve). In this mode, AltiKa successfully observes the Garonne valley without data loss and
642 does not remain locked over the hills, despite the terrain steepness (highest terrain slopes are around
643 80 m/km at 44.05°N and 100 m/km at 44.06°N).

644 Measurements for track 773 show the potential of the DEM mode to let the altimeter
645 observe a river within a steep-sided valley. Yet, this mode requires that the a priori DEM stored on
646 board has better accuracy than the size of the tracking window. For track 646, the on board DEM
647 value is almost 40 m above the actual Garonne valley elevation. This discrepancy can be related to
648 the Globcover classification, used in combination with ACE DEM, to compute on board elevations
649 (see section 2.2.2). Around virtual station SRL-646, there is no water pixel on the Garonne River in
650 Globcover (contrary to virtual station SRL-773), which biases on board elevation toward the top of

651 the hills elevation. Therefore, AltiKa loses signal over the Garonne even for cycle 1. A similar
652 discrepancy occurs with Jason-2 cycles in DEM mode. For this altimeter mission, the GMT water
653 mask used is not correctly geolocalized on the river (section 2.2.2). Thus, elevations computed
654 along the satellite track and loaded on board are also close to the top of the surrounding hills
655 elevations and not the river valley. Therefore, these cycles provide similar results to the Jason-2
656 cycles in closed-loop, which remains locked on the top of the hills for both track 070 and 035. This
657 example clearly shows DEM tracking mode sensitivity to the databases (a priori DEM and water
658 mask) used to compute the on board elevations, especially if the tracking window is smaller.

659

660 **3.3. Observation of a narrow artificial canal**

661 A frequent question asked about nadir altimetry concerns the minimum water body size that
662 can be observed with this type of altimeter. It is impossible to answer this question generally. From
663 previous examples shown in this study, it is clear that the main reasons explaining why a water body
664 is observed or not at a specific time is more linked with previous waveform history, instrument
665 settings, ground topography rather than just the water body size. The previous example of the
666 SARAL track 773 for cycle 1 on the Garonne River is a good example of such situation. All water
667 bodies within the instrument footprint that backscatter enough energy will be observed in one or
668 multiple range gates (if they are in the tracking window). In this case, the waveform will have
669 multiple peaks (with different amplitudes), corresponding to these water bodies. They could also be
670 observed on multiple consecutive waveforms along the satellite ground track. Retracker, like Ice-1
671 used in this study, use the whole waveform measured by the altimeter within the tracking window to
672 estimate one range value. Therefore, Ice-1 provides elevation for only one observed water body (the
673 first peak), but not for the others.

674 To account for the heterogeneity of the scene observed by the altimeter and all the potential
675 targets measured by the instrument, it is beneficial to plot the radargram, which corresponds to
676 waveforms recorded by the altimeter along the satellite track around a virtual station. The radargram

677 for virtual station SRL-773 during cycle 1 (in DIODE/DEM tracking mode) is shown in Figure 8.
678 This figure shows the history of the returned power along the track over the virtual station. The x-
679 axis corresponds to time (or along-track latitude) and the y-axis to the range gate number
680 (equivalent to distance). The intensity of the returned power (normalized to the maximum power
681 registered during the pass, in decibels) is shown by the color. The parabolic shapes observed on this
682 figure are characteristic of the signal returned by small size water bodies. The returned signal is
683 received by the altimeter a few kilometers before and after the satellite crosses the river. The
684 variation of distance between the river and the radar during this period explains the parabolic shape
685 (closest approach corresponds to the minimum of the parabola). Two examples of such observations
686 in Figure 8 are caused by the Garonne River and the narrow artificial canal. Two other points can
687 also be observed and correspond to very high intensity of the received signal. These points also
688 correspond to bright targets and the absence of parabola associated to them is caused by the nature
689 of the retrodiffusion by these targets: they are very specular in contrast to the two points previously
690 discussed. For more information on diffusive and specular targets responses in a radargram, see, for
691 example, Tournadre et al. (2006). Figure 2.a shows specifically SARAL track 773 for cycle 1
692 (dashed red line) and the overflowed water bodies near SRL-773 virtual stations. This specific track
693 is 1.5 km shifted compared to the nominal ENVISAT/SARAL track, due to some less stringent
694 requirement on the satellite position during the first cycles. From Figure 2.a, it is clear that the first
695 specular target and the first diffusive target corresponds to the Southernmost lake/reservoir and the
696 Garonne River mainstream (southernmost channel on this figure, which is ~150 m wide) of the
697 image, respectively. The second diffusive target, which is higher than the Garonne mainstream,
698 corresponds to the artificial canal (northernmost channel, ~70 m wide), which brings cooling water
699 to the Golfech nuclear power plant. It is less clear what the second specular target is (it could be
700 another smaller lake/reservoir, a bright man made structure like a road or metallic building roofs or
701 even another much smaller artificial canal : the “canal du Midi”). Positions of the Garonne River
702 and the Golfech canal along SARAL track are also indicated on Figure 7 (blue polygons). This

703 example clearly shows that nadir altimeters can observe small targets (river or canal with width
704 below 100 m), when the tracking window is correctly set.

705

706 **4. Conclusion and perspectives**

707 Nadir altimeters have proven their capability to observe water elevation for major rivers
708 (like the Amazon, the Congo, etc.). In this study, it has been shown they can also provide
709 meaningful water elevation for a 200 m wide, steep-sided river: the lower Garonne River in France.
710 Jason-2 time series measures water elevation with 20 cm RMSE compared to in situ observations at
711 Tonneins (115 km upstream the estuary), whereas ENVISAT mission had higher RMSE (50 cm)
712 compared to the same in situ gage. With good reason, Jason-2 10-day repeat orbit is better suited to
713 observe Garonne River seasonal cycle than the ENVISAT 35-day orbit. Therefore, Jason-2 (and to a
714 lower extent ENVISAT) repeat period seems appropriate to observe water level variations at the
715 seasonal cycle, annual, interannual and even decadal time scale (since Jason-2 was launched in
716 2008). However, Jason-2 time sampling is too coarse for observing daily/hourly high frequency
717 water level variations for this kind of medium size river. The Garonne River is very sensitive to
718 short-time intense rain events and quick snowmelt, which induces several meters water elevation
719 variations in few days and all these rapid events are missed by the satellite altimeters. Upstream
720 Tonneins, ENVISAT has higher errors and does not seem to measure water elevation as accurately
721 (Jason-2 does not sample the river upstream).

722 Comparisons between ENVISAT and in situ water elevations showed that Ice-1 retracker
723 and Sea Ice retracker provide very similar results when the Garonne River is around 200 m-wide,
724 confirming what was obtained by Sulistioadi et al. (2015). This is due to the peaky shape of the
725 waveform for small and medium size water bodies. When studying drainage basins with various
726 river widths, it would be better to use only Ice-1 altimeter heights for consistency between the
727 altimetry-based time series of water levels. Ice-1 retracking algorithm provides much better results
728 than Sea Ice over large rivers and wetlands. Ice-1-derived altimeter ranges are available in the GDR

729 for all recent altimetry missions, which is not currently the case for Sea Ice.

730 SARAL/AltiKa mostly fails to observe the river valley and remains locked on the hilly
731 surrounding areas. Such problem also happens with ENVISAT, but less often. It also happens quite
732 frequently for the Jason-2 virtual station downstream of Marmande (the other one near Tonneins is
733 less affected). This issue is related mainly to the closed-loop tracking algorithm which is influenced
734 by the history of the measurements and the geometry of observation. As a consequence, over the
735 continents, nadir altimeters tend to be locked over the top of the topography within the instrument
736 footprint and during previous measurements. This is the case over the Garonne River for
737 SARAL/AltiKa and for Jason-2 track 035, which crosses the narrow (~5 km) and steep-sided
738 Garonne River valley almost perpendicularly. However, over 30 km, Jason-2 track 70 is almost
739 parallel to the river and within the valley, which allows the closed-loop tracking mode to get locked
740 on the river. ENVISAT provides more measurements on the river, not because of a different
741 observation geometry (SARAL has the same orbit as ENVISAT), but because of differences in
742 closed-loop tracking parameters and its three tracking window sizes. Different window sizes help
743 sample a wider range span. Over the estuary, SARAL/AltiKa provides smaller RMSE (around 10
744 cm) than ENVISAT (around 30 cm) compared to tide gages.

745 To overcome challenges inherent to closed-loop tracking mode that tends to observe top of
746 the topography instead of steep-sided river, an experimental tracking mode has been developed by
747 the CNES: the DIODE/DEM mode. For SARAL/AltiKa, this experimental mode has been activated
748 only during the first cycle. Over the Garonne River, it successfully observed the Garonne valley for
749 track 773, whereas for other cycles, in closed-loop tracking mode, it failed to observe it. Yet, this
750 mode requires a priori DEM values (derived from ACE2 for SARAL) and land/water mask (derived
751 from Globcover for SARAL) to compute DEM on board along the satellite track. This on board
752 computed DEM must have vertical accuracy better than the tracking window size (which is
753 typically in the range 30-50 m, see section 2.2.2), otherwise it provides incorrect tracking
754 commands and misses the river valley (like for SARAL track 646 cycle 1 and Jason-2 track 070 and

755 035 cycles in DEM tracking mode over the Garonne). Therefore, for this tracking mode, it is crucial
756 to have an a priori, validated, database of the expected elevation for all water bodies the altimeter
757 will be forced to observe, with vertical accuracy better than the size of the tracking window. The on
758 board DEM is highly dependent of both input water mask and DEM used, which should be
759 consistent among themselves. On board DEM can be improved by using satellite imagery (e.g.
760 Landsat) for more accurate water mask, like the NARWidth database (Allen and Pavelsky, 2015).
761 For DEM values, it should be assessed if and where current global DEM are compatible with the
762 used water mask (e.g. elevations around the water mask should be lower than surrounding
763 topography in steep-sided valleys) and accurate enough. Using new (or soon to be released)
764 improved DEM, like the new version of Shuttle Radar Topography Mission (SRTM) DEM (released
765 in September 2014, see <http://www2.jpl.nasa.gov/srtm/>) or the DLR global TanDEM-X DEM (Zink
766 et al., 2014), should also improve computed on board DEM.

767 Therefore, the DIODE/DEM mode seems promising for future altimetry missions to observe
768 previously missed steep-sided rivers (or lakes). However, performance, benefits and limits of this
769 mode for continental hydrology will require more investigation by the scientific community,
770 especially because two new altimetry satellites have just been launched (Jason-3, 17 January 2016,
771 and Sentinel-3A, 16 February 2016). These altimeters are equipped with the DIODE/DEM mode
772 available along with the closed-loop tracking mode.

773

774 **Acknowledgements**

775 This project was funded by the “Réseau Thématique de Recherche Avancée - Sciences et
776 Technologies pour l’Aéronautique et l’Espace” (RTRA STAE), through a grant attributed to the
777 “Ressources en Eau sur le bassin de la GARonne : interaction entre les composantes naturelles et
778 anthropiques et apport de la téléDétection” (REGARD) project.

779 IGN, SCHAPI (especially Etienne Le Pape), DREAL Midi-Pyrénées (especially Didier
780 Narbaïs-Jaureguy), SHOM and “Grand Port Maritime de Bordeaux” (especially Alain Fort) are

781 gratefully thanked for providing freely all the DEM, in situ data and ancillary information used in
782 this study.

783 CTOH observation service at LEGOS (<http://ctoh.legos.obs-mip.fr/>) is also acknowledged
784 for processing and providing altimetry data in a uniform format for all missions.

785 CNES, ESA, ISRO and NASA are acknowledged for providing freely to the scientific
786 community measurements from the ENVISAT/RA2, Jason-2/Poseidon-3 and SARAL/AltiKa
787 altimeters.

788 Three anonymous reviewers are thanked for their constructive comments that helped to
789 improve this paper.

790

791 **References**

792 Alsdorf, D. E., and D. P. Lettenmaier. 2003. "Tracking fresh water from space." *Science* 301: 1491–
793 1494.

794

795 Allen, G. H., and T. M. Pavelsky. 2015. "Patterns of river width and surface area revealed by the
796 satellite-derived North American River Width data set." *Geophysical Research Letters* 42: 395–402.
797 doi:10.1002/2014GL062764.

798

799 Baup, F., F. Frappart, and J. Maubant. 2014. "Combining high-resolution satellite images and
800 altimetry to estimate the volume of small lakes." *Hydrology and Earth System Sciences* 18: 2007–
801 2020. doi:10.5194/hess-18-2007-2014.

802

803 Benveniste, J., M. Roca, G. Levrini, P. Vincent, S. Baker, O. Zanife, C. Zelli, and O. Bombaci.
804 2001. "The Radar Altimetry Mission: RA-2, MWR, DORIS and LRR." ESA bulletin 106: 67-76,
805 http://www.esa.int/esapub/bulletin/bullet106/bul106_5.pdf (last accessed, 19 July 2016)

806

807 Berry, P.A.M., R. Hilton, C.P.D. Johnson, and R.A. Pinnock. 2000. "ACE: a new GDEM
808 incorporating satellite altimeter derived heights". *Proceedings of the ERS-Envisat Symposium,*
809 *Gothenburg, Sweden, ESA SP-461.*, 783-791.

810

811 Berry, P. A. M., R. G. Smith, and J. Benveniste. 2010. "ACE2: the new Global Digital Elevation
812 Model." In *Gravity, Geoid and Earth Observation: IAG Commission 2: Gravity Field, Chania,*
813 *Crete, Greece, 23-27 June 2008*, edited by P. S. Mertikas, 231-237. Berlin-Heidelberg: Springer.
814 isbn: 978-3-642-10634-7. doi: 10.1007/978-3-642-10634-7_30.

815

816 Biancamaria, S., F. Hossain, and D. P. Lettenmaier. 2011. "Forecasting transboundary river water
817 elevations from space." *Geophysical Research Letters* 38: L11401. doi:10.1029/2011GL047290.

818

819 Birkett, C. M. 1995. "The contribution of TOPEX/POSEIDON to the global monitoring of
820 climatically sensitive lakes." *Journal of Geophysical Research: Oceans* 100: 25179-25204.

821

822 Birkett, C. M. 1998. "Contribution of the TOPEX NASA radar altimeter to the global monitoring of
823 large rivers and wetlands." *Water Resources Research* 34(5): 1223–1239.

824

825 Birkett, C. M., and B. Beckley. 2010. "Investigating the Performance of the Jason-2/OSTM Radar
826 Altimeter over Lakes and Reservoirs." *Marine Geodesy*, 33(S1): 204-238.
827 doi:10.1080/01490419.2010.488983.

828

829 Brown, G.S. 1977. "The average impulse response of a rough surface and its applications". IEEE
830 Transactions on Antennas and Propagation 25(1): 67-74. doi:10.1109/TAP.1977.1141536.

831

832 Cerri, L, J.-P. Berthias, W.I. Bertiger, B.J. Haines, F.G. Lemoine, F. Mercier, and J.C. Ries. 2010.

833 “Precision Orbit Determination Standards for the Jason Series of Altimeter Missions.” *Marine*
834 *Geodesy* 33(Suppl.):379-418. doi:10.1080/01490419.2010.488966.

835

836 Chelton, D.B., J.C. Ries, B.J. Haines, L.-L. Fu, and P.S. Callahan. 2001. “Satellite Altimetry”. In
837 *Satellite altimetry and Earth Sciences*, edited by Fu, L.-L. and A. Cazenave, 27-32. San Diego:
838 Academic Press.

839

840 Couhert, A., L. Cerri, J.-F. Legeais, M. Ablain, N.P. Zelensky, B.J. Haines, F.G. Lemoine, W.I.
841 Bertiger, S.D. Desai, and M. Otten. 2015. “Towards the 1 mm/y stability of the radial orbit error at
842 regional scales.” *Advances in Space Research* 55(1):2-23. doi:10.1016/j.asr.2014.06.041.

843

844 Crétaux, J. F., W. Jelinski, S. Calmant, A. V. Kouraev, V. Vuglinsk, M. Bergé Nguyen, M.-C.
845 Gennero, F. Niño, R. A. Del Rio, A. Cazenave, and P. Maisongrande. 2011. “SOLS: A lake database
846 to monitor in the Near Real Time water level and storage variations from remote sensing data”.
847 *Advances in Space Research* 47 (9): 1497-1507. doi:10.1016/j.asr.2011.01.004.

848

849 Crétaux, J.-F., S. Biancamaria, A. Arsen, M. Bergé-Nguyen, and M. Becker. 2015. “Global surveys
850 of reservoirs and lakes from satellites and regional application to the Syrdarya river basin”.
851 *Environmental Research Letters* 10(1): 015002. doi:10.1088/1748-9326/10/1/015002.

852

853 Crétaux, J.-F., R. A. Abarca-del-Río, M. Bergé-Nguyen, A. Arsen, V. Drolon, G. Clos, and P.
854 Maisongrande. 2016. “Lake Volume Monitoring from Space”. *Surveys in Geophysics* 1-37.
855 doi:10.1007/s10712-016-9362-6.

856

857 Dettmering, D., C. Schwatke, and W. Bosch. 2015. “Global Calibration of SARAL/AltiKa Using
858 MultiMission Sea Surface Height Crossovers.” *Marine Geodesy* 38(sup1):206-218.

859 doi:10.1080/01490419.2014.988832.

860

861 Desjonquères, J.D. 2009. “POSEIDON3 DEM/Diode Coupling Mode”. 2009 OSTST meeting,
862 Seattle, USA,

863 http://www.aviso.altimetry.fr/fileadmin/documents/OSTST/2009/oral/Desjonqueres_coastal.pdf

864 (last accessed, 22 July 2016)

865

866 Desjonquères, J.-D., G. Carayon , N. Steunou, and J. Lambin. 2010. “Poseidon-3 Radar Altimeter:
867 New Modes and In-Flight Performances”. *Marine Geodesy* 33(S1): 53-79.

868 doi:10.1080/01490419.2010.488970

869

870 Downing, J. A. 2010. “Emerging global role of small lakes and ponds: little things mean a lot”.
871 *Limnetica* 29(1): 9-24.

872

873 ESA. 2007. *ENVISAT RA2/MWR Product Handbook 2.2*. [http://envisat.esa.int/handbooks/ra2-](http://envisat.esa.int/handbooks/ra2-mwr/CNTR.html)
874 [mwr/CNTR.html](http://envisat.esa.int/handbooks/ra2-mwr/CNTR.html) (last accessed, 9 February 2016)

875

876 ESA. 2016. “EC/ESA COPERNICUS - SENTINEL-3C AND -3D MODELS PROCUREMENT”.
877 *ESA Intended Invitation To Tender*, A0 n°1-8197,

878 http://emits.sso.esa.int/emits/owa/emits_iitt.show_iitt?actref=15.156.03&user=Anonymous (last
879 accessed, 22 March 2016)

880

881 Frappart, F., F. Seyler, J. M. Martinez, J. G. León, and A. Cazenave. 2005. “Floodplain water
882 storage in the Negro River basin estimated from microwave remote sensing of inundation area and
883 water levels.” *Remote Sensing of Environment* 99:387-399. doi:10.1016/j.rse.2005.08.016.

884

885 Frappart, F., S. Calmant, M. Cauhopé, F. Seyler, and A. Cazenave. 2006a. “Preliminary results of
886 ENVISAT RA-2 derived water levels validation over the Amazon basin.” *Remote Sensing of the*
887 *Environment* 100(2): 252–264. doi:10.1016/j.rse.2005.10.027.

888

889 Frappart, F., K. Do Minh, J. L’Hermitte, A. Cazenave, G. Ramillien, T. Le Toan, and N. M.
890 Mognard-Campbell. 2006b. “Water volume change in the lower Mekong basin from satellite
891 altimetry and imagery data.” *Geophysical Journal International* 167(2): 570–584.
892 doi:10.1111/j.1365-246X.2006.03184.x.

893

894 Frappart, F., F. Papa, J. Santos da Silva, G. Ramillien, C. Prigent, F. Seyler, and S. Calmant. 2012.
895 “Surface freshwater storage and dynamics in the Amazon basin during the 2005 exceptional
896 drought.” *Environmental Research Letters* 7: 044010. doi:10.1088/1748-9326/7/4/044010.

897

898 Frappart, F., F. Papa, Y. Malbeteau, J. G. León, G. Ramillien, C. Prigent, L. Seoane, F. Seyler and S.
899 Calmant. 2015a. “Surface freshwater storage variations in the Orinoco floodplains using multi-
900 satellite observations.” *Remote Sensing* 7(1): 89-110. doi:10.3390/rs70100089.

901

902 Frappart, F., F. Papa, V. Marieu, Y. Malbeteau, F. Jordy, S. Calmant, F. Durand, and S. Bala. 2015b.
903 “Preliminary Assessment of SARAL/AltiKa Observations over the Ganges-Brahmaputra and
904 Irrawaddy Rivers.” *Marine Geodesy* 38(sup1): 568-580. doi:10.1080/01490419.2014.990591.

905

906 Frappart, F., C. Fatras, E. Mougin, V. Marieu, A. Diepkilé, F. Blarel, and P. Borderies. 2015c.
907 “Radar altimetry backscattering signatures at Ka, Ku, C, and S bands over West Africa”. *Physics*
908 *and Chemistry of the Earth, Parts A/B/C* 83-84: 96-110. doi:10.1016/j.pce.2015.05.001.

909

910 Getirana, A. 2010. “Integrating spatial altimetry data into the automatic calibration of hydrological

911 models”. *Journal of Hydrology* 387(3-4): 244–255. doi:10.1016/j.jhydrol.2010.04.013.

912

913 Hossain, F., A. H. M Siddique-E-Akbor., L. C. Mazumdar, S. M. Shah Newaz, S. Biancamaria, H.

914 Lee, and C. K. Shum. 2014. “Proof of concept of an operational altimeter-based forecasting system

915 for transboundary flow.” *IEEE Journal of Selected Topics in Applied Earth Observations and*

916 *Remote Sensing* 7(2): 587-601. doi:10.1109/JSTARS.2013.2283402.

917

918 Kouraev, A., E. A. Zakharov, O. Samain, N. M. Mognard-Campbell, and A. Cazenave. 2004. “Ob’

919 river discharge from Topex/Poseidon satellite altimetry.” *Remote Sensing of Environment* 93: 238-

920 245. doi:10.1016/j.rse.2004.07.007.

921

922 Laxon, S. 1994. “Sea ice altimeter processing scheme at the EODC”. *International Journal of*

923 *Remote Sensing* 15(4): 915-924.

924

925 Le Provost, C. 2001. “Ocean tides”. In *Satellite altimetry and Earth Sciences*, edited by Fu, L.-L.

926 and A. Cazenave. San Diego: Academic Press

927

928 Lee, H., C. Shum, Y. Yi, M. Ibaraki, J.-W. Kim, A. Braun, C.-Y. Kuo, and Z. Lu. 2009. “Louisiana

929 wetland water level monitoring using retracked TOPEX/POSEIDON altimetry.” *Marine Geodesy*

930 32: 284-302. doi:10.1080/01490410903094767.

931

932 Legrésy, B., and F. Rémy. 1997. “Surface characteristics of the Antarctic ice sheet and altimetric

933 observations”. *Journal of Glaciology* 43(144): 197-206.

934

935 León, J.G., S. Calmant, F. Seyler, M. P. Bonnet, M. Cauhopé, F. Frappart, N. Filizola, and P. Fraizy.

936 2006. “Estimation of stage-discharge rating curves and mean water depths from radar altimetry data

937 and hydrological modelling in the upper Negro River basin.” *Journal of Hydrology* 328(3-4): 481-
938 496. doi:10.1016/j.jhydrol.2005.12.006.

939

940 Martin, E., S. Gascoin, Y. Grusson, C. Murgue, M. Bardeau, F. Ancil, S. Ferrant, R. Lardy, P. Le
941 Moigne, D. Leenhardt, V. Rivalland, J.-M. Sánchez Pérez, S. Sauvage, and O. Therond. 2016. “On
942 the use of hydrological models and satellite data to study the water budget of river basins affected
943 by human activities: examples from the Garonne basin of France.” *Surveys in Geophysics* 37(2):
944 223-247. doi:10.1007/s10712-016-9366-2.

945

946 Medina, C. E., J. Gomez-Enri, J. J. Alonso, and P. Villares. 2008. “Water level fluctuations derived
947 from ENVISAT Radar Altimeter (RA-2) and in situ measurements in a subtropical waterbody: Lake
948 Izabal (Guatemala).” *Remote Sensing of Environment* 112(9): 3604-3617.
949 doi:10.1016/j.rse.2008.05.001.

950

951 Meybeck, M., G. Friedrich, R. Thomas, and D. Chapman. 1996. “Chapter 6 - Rivers.” In *Water*
952 *Quality Assessments – a Guide to Use of Biota, Sediments and Water in Environmental Monitoring*,
953 2nd Edn., edited by D. Chapman, UNESCO/WHO/UNEP, 247-248. London-New York: Taylor and
954 Francis.

955

956 Michailovsky, C. I., S. McEnnis, P. A. M. Berry, R. Smith, and P. Bauer-Gottwein. 2012. “River
957 monitoring from satellite radar altimetry in the Zambezi River basin.” *Hydrology and Earth System*
958 *Sciences* 16: 2181–2192. doi:10.5194/hess-16-2181-2012.

959

960 Michailovsky, C. I., and P. Bauer-Gottwein. 2014. “Operational reservoir inflow forecasting with
961 radar altimetry: the Zambezi case study.” *Hydrology and Earth System Sciences* 18(3): 997-1007.
962 doi:10.5194/hess-18-997-2014.

963

964 Moriasi, D.N. , J. G. Arnold, M. W. Van Liew, R. L. Bingne, R. D. Harmel, and T. L. Veith. 2007.
965 “Model evaluation guidelines for systematic quantification of accuracy in watershed simulations.”
966 *Transactions of the ASABE* 50(3): 885-900.

967

968 Nash, J. E., and J. V. Sutcliffe. 1970. “River flow forecasting through conceptual models part I-A
969 discussion of principles.” *Journal of Hydrology* 10(3): 282-290. doi:10.1016/0022-1694(70)90255-
970 6.

971

972 Paiva, R. C. D., D. C. Buarque, W. Colischonn, M.-P. Bonnet, F. Frappart, S. Calmant, and C. A. B.
973 Mendes. 2013. “Large-scale hydrological and hydrodynamics modelling of the Amazon River
974 basin.” *Water Resources Research* 49(3):1226-1243. doi:10.1002/wrcr.20067.

975

976 Papa, F., S. K. Bala, R. Kumar Pandey, F. Durand, A. Rahman, and W. B. Rossow. 2012. “Ganga-
977 Brahmaputra river discharge from Jason-2 radar altimetry: an update to the long-term satellite-
978 derived estimates of continental freshwater forcing flux into the Bay of Bengal.” *Journal of*
979 *Geophysical Research* 117: C11021. doi:10.1029/2012JC008158.

980

981 Pfeffer, J. , F. Seyler, M.-P. Bonnet, S. Calmant, F. Frappart, F. Papa, R. C. D. Paiva, F. Satgé, and J.
982 Santos da Silva. 2014. “Low-water maps of the groundwater table in the central Amazon by satellite
983 altimetry.” *Geophysical Research Letters* 41: 1981–1987. doi:10.1002/2013GL059134.

984

985 Ponchaut, F., and A. Cazenave. 1998. “Continental lake level variations from Topex/poseidon
986 (1993-1996).” *Comptes Rendus de l’Académie des Sciences Series IIA Earth and Planetary Science*
987 326(1): 13-20.

988

989 Ricko, M., C. Birkett, J. A. Carton, and J.-F. Crétaux. 2012. “Intercomparison and validation of
990 continental water level products derived from satellite radar altimetry.” *Journal of Applied Remote*
991 *Sensing* 6(1): 061710. doi:10.1117/1.JRS.6.061710.

992

993 Santos da Silva, J., S. Calmant, F. Seyler, O. Corrêa Rotunno Filho, G. Cochonneau, and
994 W. J. Mansur. 2010. “Water levels in the Amazon basin derived from the ERS 2 and ENVISAT
995 radar altimetry missions.” *Remote Sensing of Environment* 114: 2160–2181.
996 doi:10.1016/j.rse.2010.04.020.

997

998 Sauquet, E, A. Dupeyrat, F. Hendrickx, C. Perrin, R. Samie, J.-P. Vidal. 2009. *IMAGINE 2030,*
999 *climat et aménagements de la Garonne : quelles incertitudes sur la ressource en eau en 2030 ?*
1000 [IMAGINE 2030, climate and water management: uncertainties on water resources for the Garonne
1001 river basin in 2030?]. Lyon: Irstea Publications. [http://cemadoc.irstea.fr/oa/PUB00028876-imagine-](http://cemadoc.irstea.fr/oa/PUB00028876-imagine-2030-climat-amenagements-garonne-queelles-i.html)
1002 [2030-climat-amenagements-garonne-queelles-i.html](http://cemadoc.irstea.fr/oa/PUB00028876-imagine-2030-climat-amenagements-garonne-queelles-i.html) (last accessed 23 February 2016).

1003

1004 Scharroo, R., H. Bonekamp, C. Ponsard, F. Parisot, A. von Engeln, M. Tahtadjiev, K. de Vriendt,
1005 and F. Montagner. 2015. “Jason continuity of services: continuing the Jason altimeter data records
1006 as Copernicus Sentinel-6.” *Ocean Science Discussion* 12: 2931-2953. doi:10.5194/osd-12-2931-
1007 2015.

1008

1009 Sengenès, P., and N. Steunou. 2011. “SARAL/ALTIKA”. 2011 OSTST meeting, San Diego, USA,
1010 [http://www.aviso.oceanobs.com/fileadmin/documents/OSTST/2011/oral/03_Friday/Plenary/New%2](http://www.aviso.oceanobs.com/fileadmin/documents/OSTST/2011/oral/03_Friday/Plenary/New%20Frontiers/05%20Pierre%20SARAL-Altika%20San%20Diego%20OSTST%202011%2021-10-2011.pdf)
1011 [0Frontiers/05%20Pierre%20SARAL-Altika%20San%20Diego%20OSTST%202011%2021-10-](http://www.aviso.oceanobs.com/fileadmin/documents/OSTST/2011/oral/03_Friday/Plenary/New%20Frontiers/05%20Pierre%20SARAL-Altika%20San%20Diego%20OSTST%202011%2021-10-2011.pdf)
1012 [2011.pdf](http://www.aviso.oceanobs.com/fileadmin/documents/OSTST/2011/oral/03_Friday/Plenary/New%20Frontiers/05%20Pierre%20SARAL-Altika%20San%20Diego%20OSTST%202011%2021-10-2011.pdf) (last accessed, 22 July 2016)

1013

1014 Steunou, N., J.-D. Desjonquères, N. Picot, P. Sengenès, J. Noubel, and J. C. Poisson. 2015. “AltiKa

1015 Altimeter: Instrument Description and In Flight Performance.” *Marine Geodesy* 38(sup1): 22-42.
1016 doi: 10.1080/01490419.2014.988835.
1017

1018 Sulistioadi, Y. B., K.-H. Tseng, C. K. Shum, H. Hidayat, M. Sumaryono, A. Suhardiman, F.
1019 Setiawan, and S. Sunarso. 2015. “Satellite radar altimetry for monitoring small rivers and lakes in
1020 Indonesia.” *Hydrology and Earth System Sciences* 19: 341-359. doi:10.5194/hess-19-341-2015.
1021

1022 Tarpanelli, A., L. Brocca, S. Barbeta, M. Faruolo, T. Lacava, and T. Moramarco. 2015. “Coupling
1023 MODIS and radar altimetry data for discharge estimation in poorly gauged river basins.” *IEEE*
1024 *Journal of Selected Topics in Applied Earth Observations and Remote Sensing* 8(1): 141-148.
1025 doi:10.1109/JSTARS.2014.2320582.
1026

1027 Tournadre, J., B. Chapron, N. Reul, and D. C. Vandemark. 2006. “A satellite altimeter model for
1028 ocean slick detection.” *Journal of Geophysical Research* 111:C04004. doi:10.1029/2005JC003109.
1029

1030 Verpoorter, C., T. Kutser, D. A. Seekell, and L. J. Tranvik. 2014. “A global inventory of lakes based
1031 on high-resolution satellite imagery.” *Geophysical Research Letters* 41: 6396–6402.
1032 doi:10.1002/2014GL060641.
1033

1034 Wilson, M.D., P. D. Bates, D. E. Alsdorf, B. Forsberg, M. Horrit, J. Melack, F. Frappart, J. S.
1035 Famiglietti. 2007. “Modeling large-scale inundation of Amazonian seasonally flooded wetlands.”
1036 *Geophysical Research Letters* 34: L15404. doi:10.1029/2007GL030156.
1037

1038 Wingham, D.J., C. G. Rapley, and H. Griffiths. 1986. “New techniques in satellite altimeter
1039 tracking systems”. In *Proceedings of IGARSS’86 Symposium, Zürich, 8–11 September*
1040 *1986*, edited by ESA, SP-254: 1339–1344.

1041

1042 Yamazaki, D., H. Lee, D. E. Alsdorf, E. Dutra, H. Kim, S. Kanae, and T. Oki. 2012. “Analysis of
1043 the water level dynamics simulated by a global river model: A case study in the Amazon River.”
1044 *Water Resources Research* 48: W09508. doi:10.1029/2012WR011869.

1045

1046 Zelli, C. 1999. “ENVISAT RA-2 advanced radar altimeter: instrument design and prelaunch
1047 performance assessment review.” *Acta Astronautica* 44 (7): 323–333. doi:10.1016/S0094-
1048 5765(99)00063-6.

1049

1050 Zink, M., M. Bachmann, B. Bräutigam, T. Fritz, I. Hajsek, A. Moreira, B. Wessel, G. Krieger.
1051 2014. “TanDEM-X: The new global DEM takes shape.” *IEEE Geoscience and Remote Sensing*
1052 *Magazine*, 2 (2), 8-23. doi:10.1109/MGRS.2014.2318895.

1053

1054 **Tables**

1055 Table 1. Altimetry missions used in this study and their main characteristics

	Altimetry missions used		
Mission name	ENVISAT	Jason-2	SARAL
Operating agencies	ESA	CNES, EUMETSAT, NASA, NOAA	CNES, ISRO
Mission duration	2002 - 2010 on the nominal orbit (below)	2008 - present	2013 - present
Orbit repeat period	35 days	10 days	35 days
Orbit altitude	790 km	1336 km	790 km
Orbit inclination	98.54°	66°	98.54°
Equatorial ground-track distance	80 km	315 km	80 km
Altimeter name	RA-2	Poseidon-3	AtiKa
Radar frequencies	Ku- and S-bands	Ku- and C-bands	Ka-band
Range window size	64 m, 256 m, 1024 m	50 m	30 m
Number of used range window bins	104	104	104
Along track sampling	18 Hz (~400 m)	20 Hz (~350 m)	40 Hz (~175 m)
DEM tracking mode	No	Yes	Yes
DEM used for DEM mode	-	ACE	ACE2
Cycle(s) in DEM tracking mode	-	3, 5, 7, 34, 209, 220	1

1056

1057

1058 Table 2. Satellite altimetry virtual stations name, closest in situ gage name, number of common
 1059 dates in the altimetry and in situ time series, correlation coefficient, mean bias and RMSE between
 1060 altimetry and in situ water elevation time series, RMSE and Nash-Sutcliffe coefficient between
 1061 altimetry and in situ water elevation anomaly time series, and amplitude (maximum minus
 1062 minimum) of the in situ water elevation time series at the common dates, along the Garonne River
 1063 mainstream (from upstream to downstream virtual stations).

1064

Alti virtual station (+ length river crossing)	In situ gage (+ river width in m)	Dist alti/gage (km)	Nb dates alti/ in situ	Corr coeff	Mean bias (m)	RMSE (m)	Anom RMSE (m)	Anom NS coeff	In situ amplitude (m)
ENV-102 (250 m)	Verdun-sur-Garonne (130 m)	29.5	48	0.41	27.90	27.92	0.95	-3.10	1.56
ENV-773 (130 m)	Lamagistère (150 m)	10.5	46	0.35	8.66	8.80	1.55	-2.63	3.52
SRL-773 (130 m)	Lamagistère (150 m)	10.5	6	-0.80	105.10	105.13	2.56	-3.88	3.29
ENV-646 (175 m)	Lamagistère (150 m)	1.4	64	0.62	1.61	1.80	0.81	-0.53	2.60
SRL-646 (175 m)	Lamagistère (150 m)	1.4	6	-0.14	103.53	103.55	2.01	-2.00	3.29
ENV-188 (700 m)	Tonneins (200 m)	2.5	70	0.85	-0.23	0.58	0.53	0.73	3.83
SRL-188 (700 m)	Tonneins (200 m)	2.5	11	0.90	-1.77	1.90	0.69	0.80	5.3
JA2-070 (185 m)	Tonneins (200 m)	5.3	165	0.98	-2.56	2.57	0.22	0.95	4.41
JA2-070 (185 m)	Marmande (200 m)	9.2	150	0.98	4.04	4.04	0.20	0.96	4.20
ENV-315 (2 km)	Marmande (200 m)	14.2	21	0.81	-1.27	1.41	0.59	0.66	3.43
SRL-315 (2 km)	Marmande (200 m)	14.2	4	-0.84	44.15	44.19	1.97	-1.36	3.48
JA2-035 (160 m)	Marmande (200 m)	30	62	0.91	-6.95	6.96	0.36	0.82	3.74

1065

1066

1067

1068

1069

1070 Table 3. Correlation coefficient, RMSE (in meter) and Nash-Sutcliffe coefficient between water
 1071 elevation anomaly time series for ENVISAT altimetry and the closest in situ gage (see Table 2),
 1072 along the Garonne River mainstream (from upstream to downstream virtual stations). The
 1073 comparison is done for two retracker algorithms (Ice-1 and Sea Ice) and using rather the median or
 1074 the mean of retracked points within the virtual station per observation time. In bold number
 1075 correspond to the better result obtain for each virtual station and each statistic.

		ENVISAT virtual stations				
		ENV-102	ENV-773	ENV-646	ENV-188	ENV-315
Corr coeff	Median Ice-1	0.42	0.35	0.63	0.85	0.82
	Mean Ice-1	0.41	0.35	0.62	0.85	0.84
	Median Sea Ice	0.50	0.33	0.65	0.88	0.79
	Mean Sea Ice	0.50	0.33	0.65	0.87	0.80
Anom RMSE (m)	Median Ice-1	0.95	1.55	0.81	0.53	0.59
	Mean Ice-1	0.94	1.55	0.80	0.54	0.57
	Median Sea Ice	0.89	1.80	0.70	0.51	0.63
	Mean Sea Ice	0.89	1.80	0.69	0.51	0.61
Anom NS coeff	Median Ice-1	-3.10	-2.63	-0.53	0.73	0.66
	Mean Ice-1	-3.01	-2.63	-0.48	0.72	0.69
	Median Sea Ice	-2.60	-3.90	-0.12	0.76	0.62
	Mean Sea Ice	-2.60	-3.90	-0.09	0.75	0.65

1076

1077

1078 Table 4. Satellite altimetry virtual stations name, closest tide gage name, number of common dates
 1079 in the altimetry and in situ time series, correlation coefficient, mean bias and RMSE between

1080 altimetry and in situ water elevation time series, RMSE and Nash-Sutcliffe coefficient between
 1081 altimetry and in situ water elevation anomaly time series, and amplitude (maximum minus
 1082 minimum) of the in situ water elevation time series at the common dates, along the Gironde estuary.

1083

Alti virtual station	Tide gage	Dist alti/gage (km)	Nb dates alti/ in situ	Corr coeff	Mean bias (m)	RMSE (m)	Anom RMSE (m)	Anom NS coeff	In situ amplitude (m)
ENV-274	Richard	6.5	35	0.28	-	-	1.51	-0.91	5.26
SRL-274	Richard	6.5	15	0.09	-	-	1.57	-0.21	4.54
ENV-859	Royan	5.0	17	0.98	1.01	1.06	0.31	0.94	3.76
SRL-859	Royan	5.0	15	0.99	0.32	0.34	0.09	0.99	3.27
ENV-859	Port-Bloc	3.7	39	0.97	0.73	0.78	0.26	0.94	3.55
SRL-859	Port-Bloc	3.7	15	0.99	0.14	0.20	0.13	0.98	3.26

1084

1085

1086

1087

1088

1089

1090

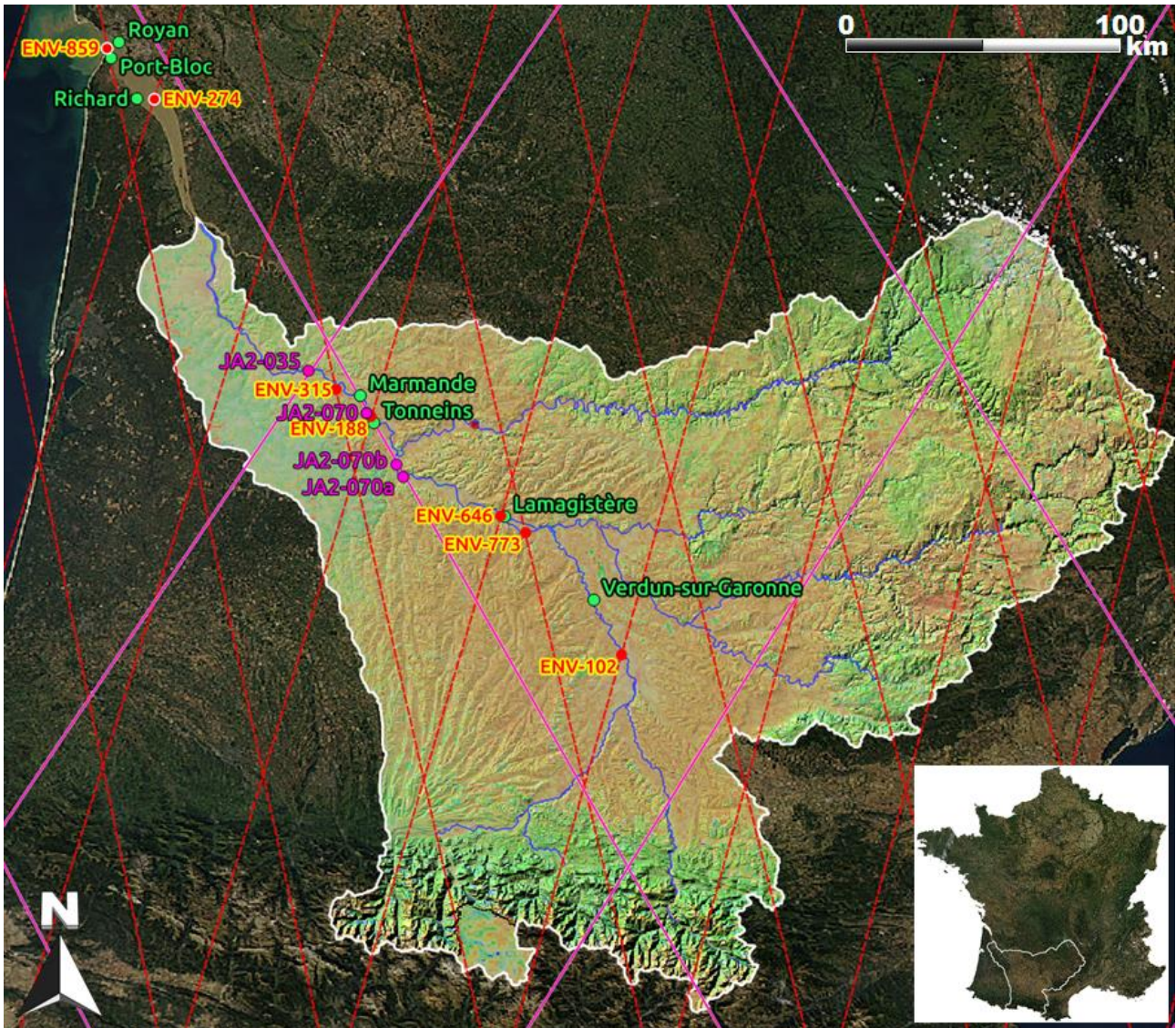
Table 5. Percentage of data, for all ENVISAT cycles, acquired in each tracking mode, for all virtual stations. 320 MHz, 80 MHz and 20 MHz tracking modes correspond to a tracking window size of 64 m, 256 m and 1024 m, respectively.

		ENVISAT virtual stations						
		ENV-102 (river)	ENV-315 (river)	ENV-773 (river)	ENV-646 (river)	ENV-188 (river)	ENV-274 (estuary)	ENV-859 (estuary)
ENVISAT tracking modes	320 MHz	28	77	44	76	80	96	100
	80 MHz	71	22	33	23	19	3	0
	20 MHz	0	1	23	1	1	1	0

1091

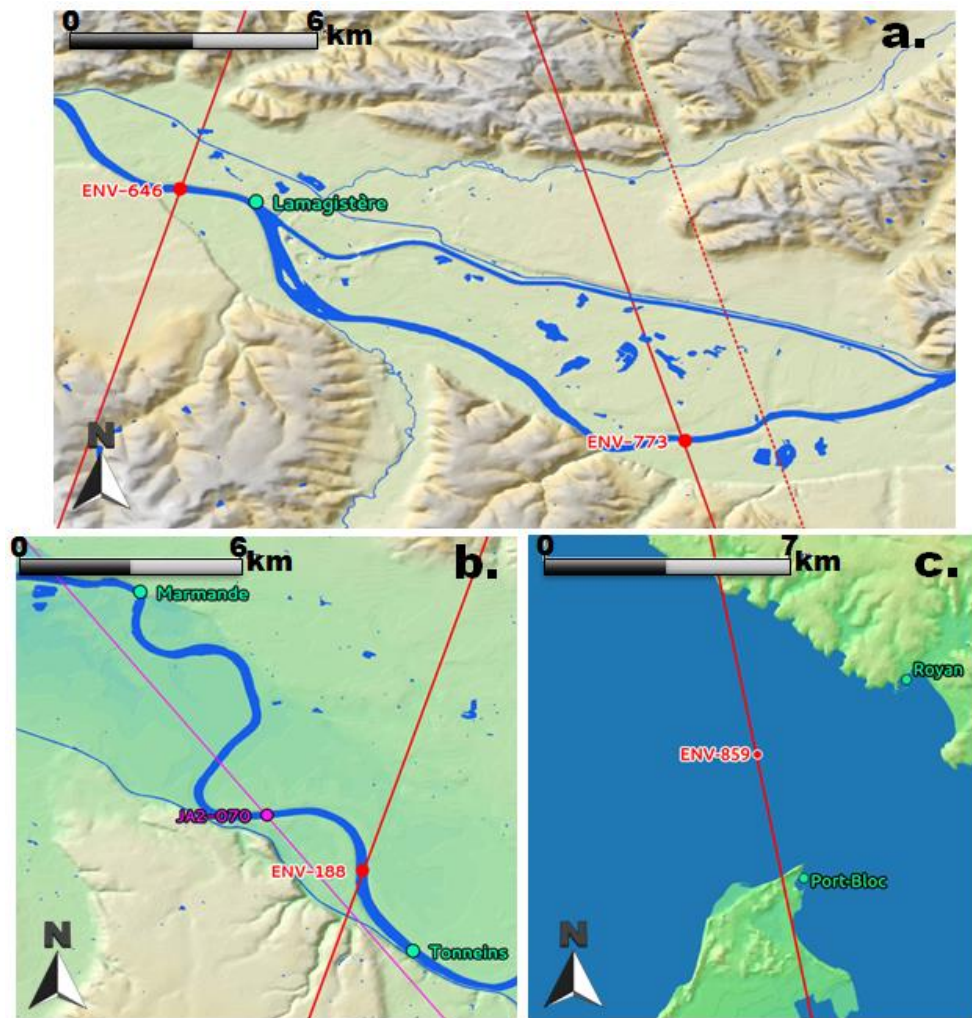
1092
1093
1094
1095

Figures



1096

Figure 1. Garonne basin (white boundaries), with in situ gages (green dots), ENVISAT and SARAL virtual stations (red dots) and Jason-2 virtual stations (magenta dots) used in this study. Dotted red lines correspond to ENVISAT and SARAL ground tracks. Magenta lines correspond to Jason-2 ground tracks. Background colors correspond to a MODIS image from 01 October 2011, whose color has been artificially lightened using a shaded relief, computed from a DEM provided by IGN, over the Garonne basin. Location of the Garonne basin in France main territory is shown in the bottom right hand corner map (white boundaries)



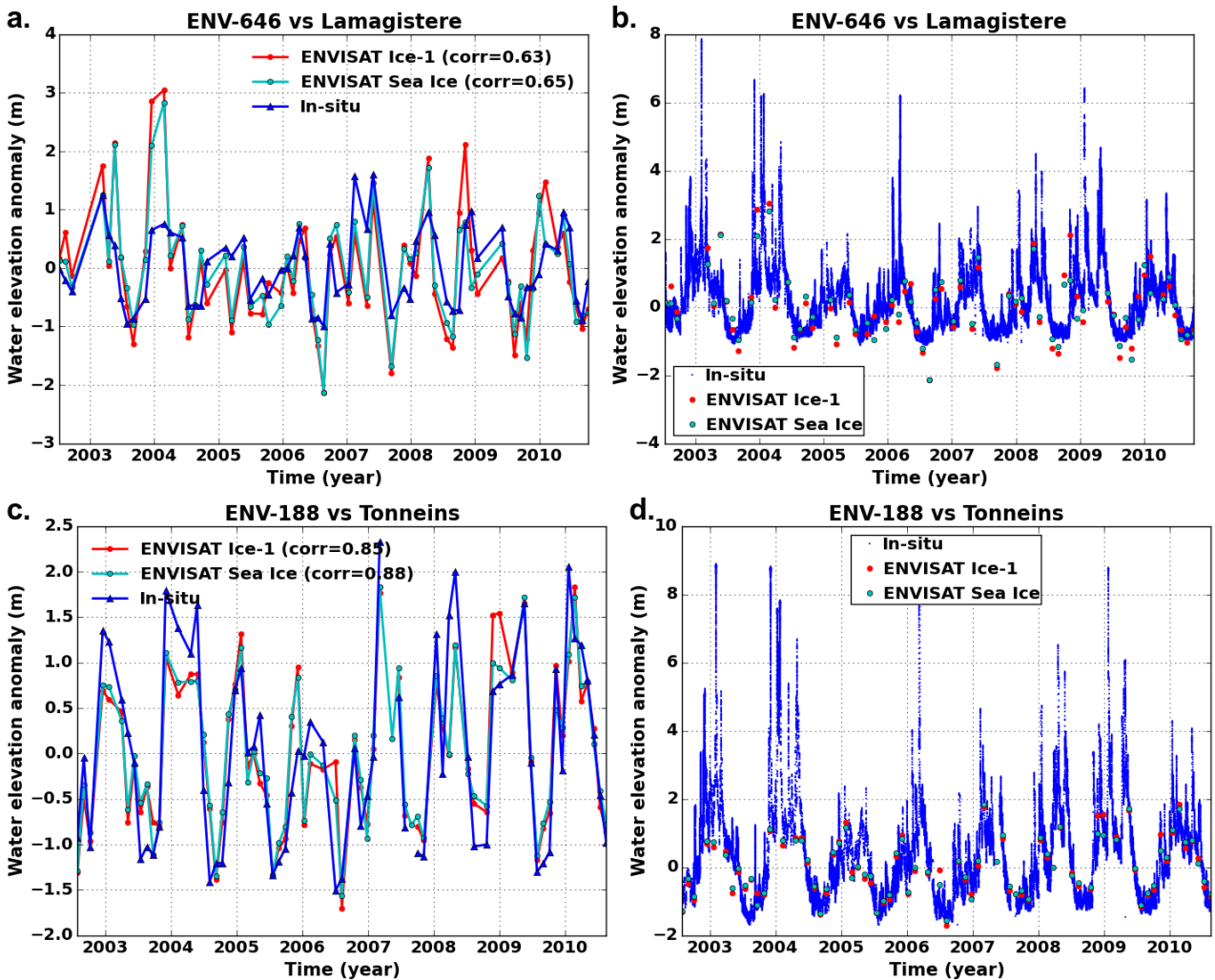
1097

1098 *Figure 2. ENVISAT satellite nominal ground tracks (red line), ENVISAT virtual stations (red dots),*

1099 *Jason-2 satellite nominal ground track (magenta), Jason-2 virtual stations (magenta dot) and in*

1100 *situ gages (green dots) over the Garonne mainstream at Lamagistère (a.), Tonneins (b.) and over*

1101 *the estuary (c.). Dashed red line on panel (a.) corresponds to SARAL ground track 773 for cycle 1*



1102

1103

Figure 3. ENVISAT water elevation anomaly computed with Ice-1 retracker (red line on panels a.

1104

and c. and red dots on panels b. and d.) and with Sea Ice retracker (cyan line on panels a. and c.

1105

and cyan dots on panels b. and d.), in situ water elevation anomaly at ENVISAT measurement times

1106

(blue line on panels a. and c.) and all records in the in situ water elevation anomaly time series

1107

between 2003 and 2010 (blue dots on panels b. and d.) for virtual station 646 and Lamagistère gage

1108

(panels a. and b.) and virtual station 188 and Tonneins gage (panels c. and d.). In these panels,

1109

water elevation anomaly time series correspond to water elevations minus the time series temporal

1110

mean over the same common dates between in situ and altimetry time series. The term 'corr'

1111

corresponds to the altimetry time series and the corresponding in situ time series correlation

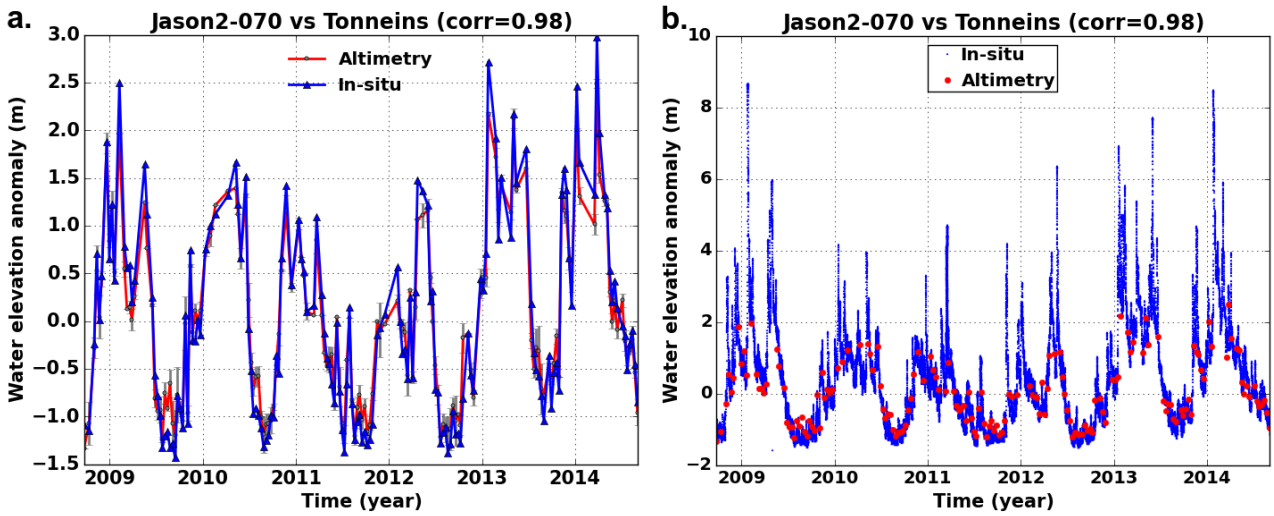
1112

coefficient. For more statistics concerning these virtual stations, see Table 2

1113

1114

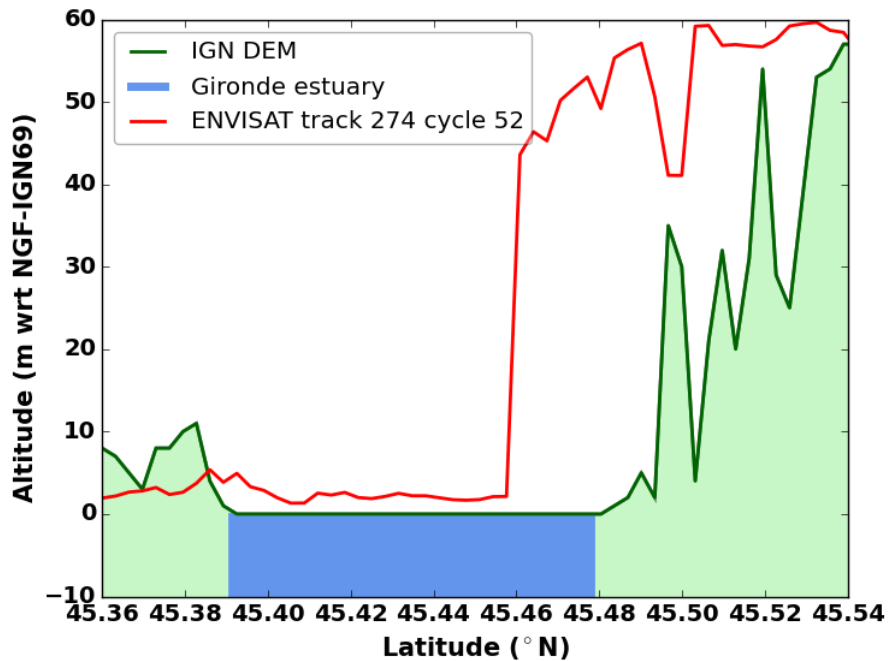
1115



1116

1117 *Figure 4. Jason-2 virtual station 070 water elevation anomaly (red line on panel a. and red dots on*
 1118 *panel b.) and in situ water elevation anomaly measured by the Tonneins gage at Jason-2*
 1119 *measurement times (blue line on panel a.) and all records in the in situ water elevation anomaly*
 1120 *time series between 2003 and 2010 (blue dots on panel b.)*

1121

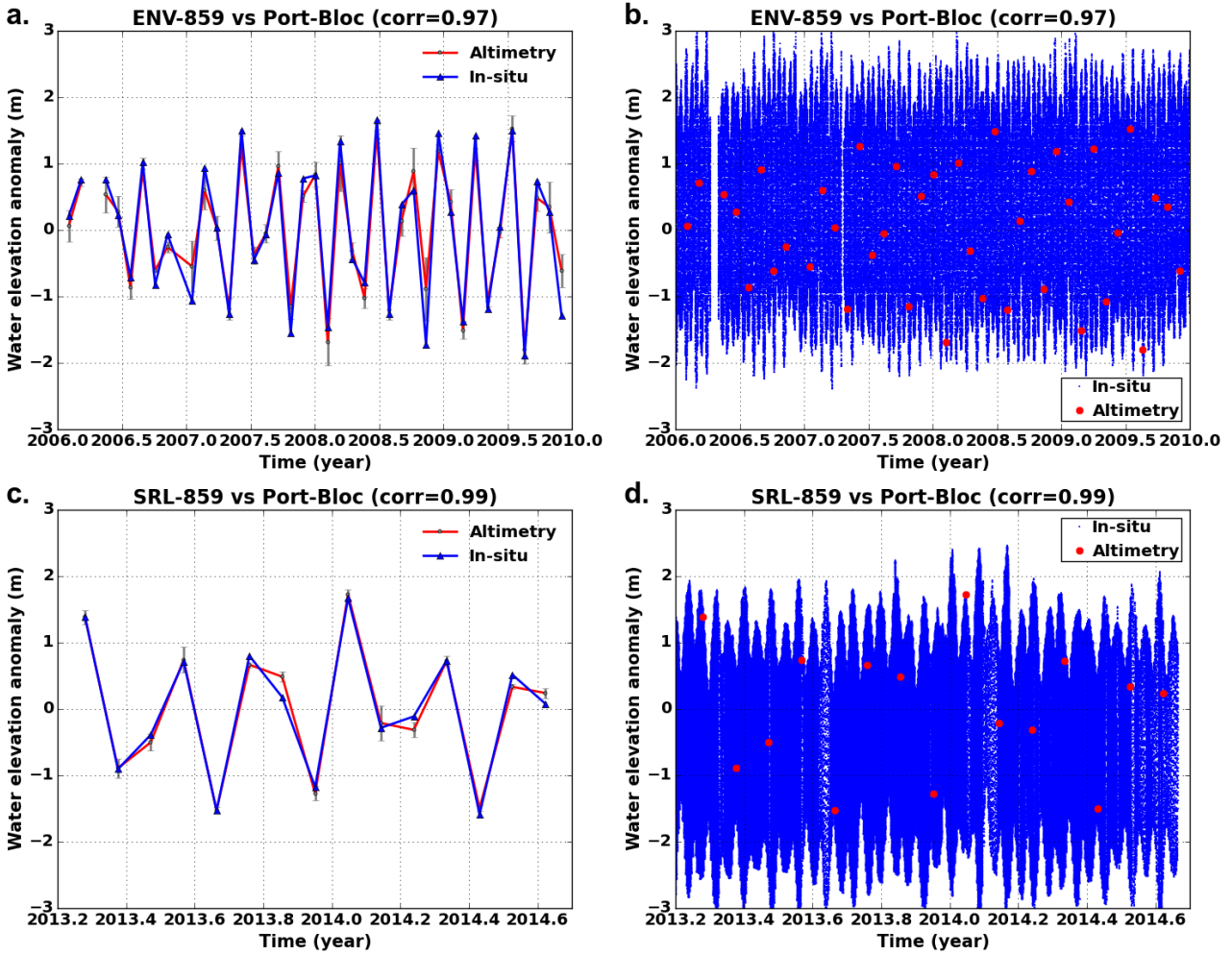


1122

1123 *Figure 5. Comparison between IGN DEM (green line) along the ENVISAT 274 track (see Figure 1)*
 1124 *over the Gironde estuary (its position is shown by the light blue polygon, its elevation corresponds*
 1125 *to the DEM and not to the actual water level) and elevation measured by ENVISAT for cycle 59 (21*

1126 June 2007, red curve)

1127



1128

1129 Figure 6. Comparison between virtual station 859 water elevation anomaly (red line on panels a.

1130 and c. and red dots on panels b. and d.), water elevation anomaly register by the Port-Bloc tide

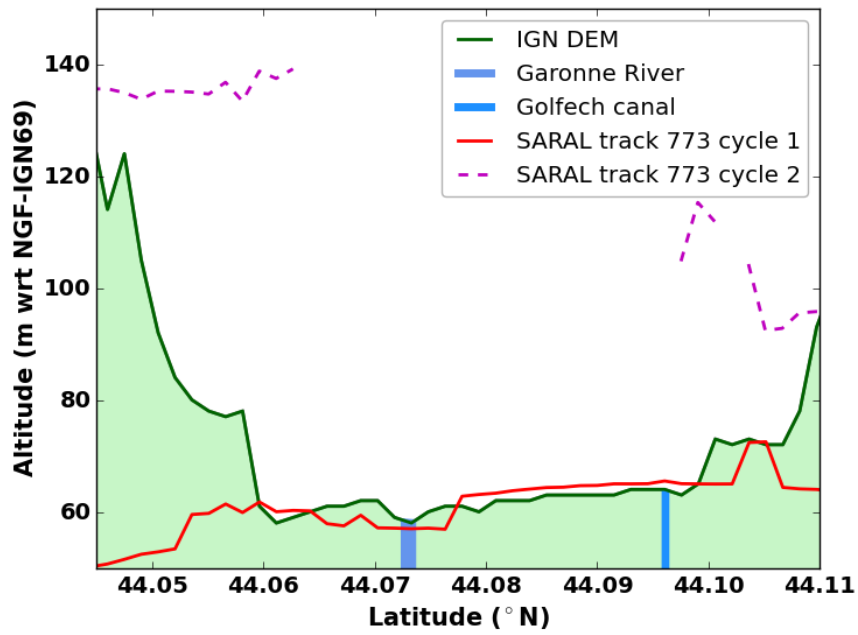
1131 gage (blue line on panels a. and c.) at altimeter measurement times and all tide gage measurements

1132 (blue dots on panels b. and d.) for ENVISAT between 2006 and 2010 (panels a. and b.) and for

1133 Saral between 2013 and 2014 (panels c. and d.)

1134

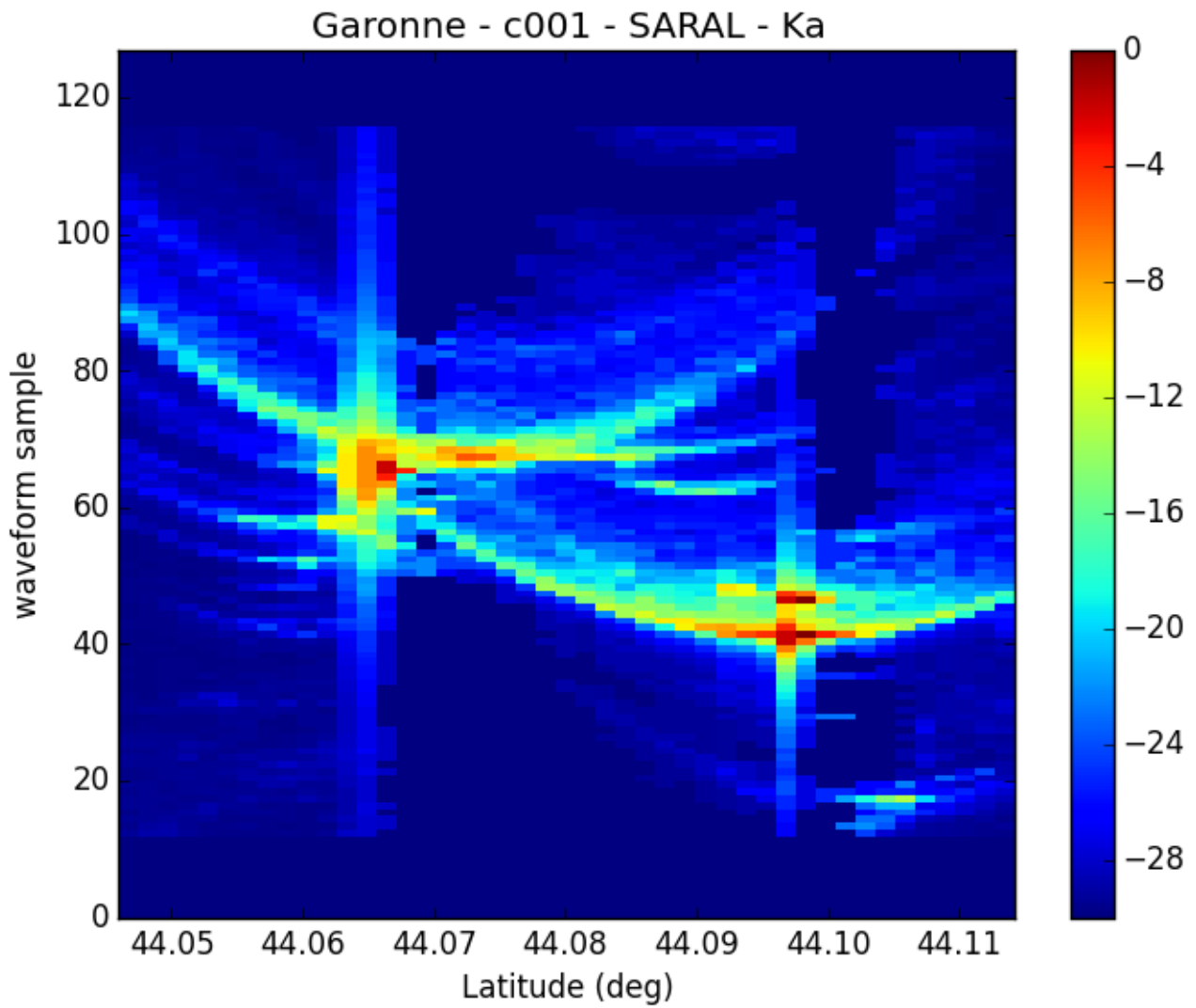
1135



1136

1137 *Figure 7. Comparison between IGN DEM (green line) along the SARAL 773 track (see Figure 1)*
 1138 *over the Garonne River (its position is shown by the large blue polygon near 44.07°N, its elevation*
 1139 *corresponds to the DEM and not to the actual river water level) and the artificial canal (tight light*
 1140 *blue polygon near 44.09°N), elevations measured by SARAL/AltiKa for cycle 1 (10 April 2013, red*
 1141 *curve) and for cycle 2 (15 May 2013, dashed magenta curve)*

1142



1143

1144 *Figure 8. Radargram for SARAL/AltiKa cycle 1 pass over virtual station SRL-773. This is a*
 1145 *representation of the successive waveforms measured on this pass. Each column represents one*
 1146 *waveform (y-axis correspond to range gates number). Colors represent returned power received in*
 1147 *each bin. A logarithmic scale (decibels) is used in order to be able to represent the large dynamic of*
 1148 *received power.*